NEWTON

HORIZON 2020
THE FRAMEWORK PROGRAMME FOR RESEARCH AND INNOVATION

NEWTON Deliverable D3.6

Final Design Report: NEWTON instrument prototype 3

Project Number:	**730041**
Project Title	**New portable multi-sensor scientific instrument for non-invasive on-site characterisation of rock from planetary surface and sub-surfaces.**
Deliverable Type:	**Public**

Title:	D3.6 - Final Design Report: NEWTON instrument prototype 3
Work Package:	Work Package 3
Responsible:	TTI
Due Date:	30.04.2018
Nature:	Report
Security:	Public
Version:	1.0

Authors:
TTI: Cristina Lavín, Laura González , Reinel Marante
INTA: Marina Díaz, José Luis Mesa, Javier de Frutos, Miguel Ángel Rivero, Amanda Ordoñez, Veracruz González
UPM: Claudio Aroca, Mar Sanz, Marco Maicas, Marina Pérez, Pedro Cobos
UT: Rolf Kilian

Abstract: As it is included in NEWTON DoA, D3.6- Final design and validation report for the power distribution block should describe the final design and validation of the power distribution block. However, during the first NEWTON periodic review it was agreed to modify the content and objectives of deliverables D3.4, D3.5 and D3.6 and to include in each of them the final design of NEWTON prototypes 1, 2 and 3 respectively. This was requested with the aim of improving the comprehensibility of the documents and the activities developed for the completion of the final design of each instrument. Due to this reason, this document, renamed as D3.6 - Final Design Report: NEWTON instrument prototype 3, describes the final design of the NEWTON instrument prototype 3, as well as the functional verification of its key building blocks, i.e. sensor head, electronic control unit and the power distribution unit.

Keyword list: Planetary Science, complex susceptibility, multi-sensor system, Mars, the Moon, control unit, lock-in, signal processing, susceptometer, magnetometer, magnetic amplifier.

Executive Summary

As it is included in NEWTON DoA, D3.6- Final design and validation report for the power distribution block should describe the final design and validation of the power distribution block. However, during the first NEWTON periodic review it was agreed to modify the content and objectives of deliverables D3.4, D3.5 and D3.6 and to include in each of them the final design of NEWTON prototypes 1, 2 and 3 respectively. This was requested with the aim of improving the comprehensibility of the documents and the activities developed for the completion of the final design of each instrument. Due to this reason, this document, renamed as D3.6 - Final Design Report: NEWTON instrument prototype 3, describes the final design of the NEWTON instrument prototype 3, as well as the functional verification of its key building blocks.

With the aim of maximizing the impact of novel NEWTON technology, different prototypes are being developed within the project. Two prototypes (named prototype 1 and 3) are being developed for planetary application, while a slightly (reduced) adapted version of prototype 1 (named prototype 2) will be developed in order to demonstrate the spin-off of the technology between space and non-space fields. The three prototypes share the same architecture while they provide different performance capabilities adapted to different scenarios. The key building blocks of the three prototypes are the same, i.e. Power Distribution Unit (PDU), the electronic Control Unit (CU) and the Sensor Unit (SU). As already indicated, this document reports the final design of prototype 3, as well as the functional verification of its Sensor Unit, electronic Control Unit and Power Distribution Unit, while D3.4 and D3.5 describe the final design of NEWTON prototype 1 and 2 respectively, as well as the functional verification of their respective key blocks.

This document is structured in different sections. Section 2 gives an overview of the architecture and main features of NEWTON instrument prototype 3. Section 3, 4 and 5 describe respectively the final design of the sensor unit, electronic control unit and power distribution unit. The functional verification of each key building block is also included in the respective section. Finally, Section 6 presents a summary of the content included in this document, the main conclusions on the degree of advance obtained from it as well as the future lines of work, while Section 7 provides the referenced bibliography.

Authors

Partner	Name	Email
TTI	Cristina Lavín	clavin@ttinorte.es
	Laura González	lgonzalez@ttinorte.es
	Reinel Marante	rmarante@ttinorte.es
INTA	Marina Díaz	diazma@inta.es
	José Luis Mesa	mesaujl@inta.es
	Javier de Frutos	frutosfj@inta.es
	Miguel Ángel Rivero	riveroma.pers_externo@inta.es
	Amanda Ordoñez	arlensiuoca@inta.es
	Veracruz González	gonzalezgv@inta.es
UPM	Claudio Aroca	claudio.aroca@upm.es
	Mar Sanz	mar.sanz.lluch@upm.es
	Marco Maicas	marco.maicas@upm.es
	Marina Pérez	marina.perez@isom.upm.es
	Pedro Cobos	pedro.cobos@upm.es
UT	Rolf Kilian	kilian@uni-trier.de

Table of Contents

Abbreviations

A	Ampere
AC	Alternating Current
ADC	Analog to Digital Converter
ACK	Acknowledgement
AMR	Anisotropic Magneto Resistance
ARM	Anhysteretic Remanence Measurements
B	Magnetic Induction
C	Capacitance
CRC	Cyclic Redundancy Code
CU	Control Unit
D	Deliverable
DAC	Digital to Analog Converter
DC	Direct Current
DoA	Description of Action
DSP	Digital Signal Processor
EMF	Electromotive Force
FEM	Finite Element Method
INTA	Instituto Nacional Técnica Aeroespacial “Esteban Terradas”
IRM	Isothermal Remanent Magnetization
LSB	Least Significant Byte
M	Magnetization
MOSFET	Metal-Oxide Semiconductor Field-Effect Transistor
MSB	Most Significant Byte
NRM	Natural Remanent Magnetization
PC	Personal Computer
PCB	Printed Circuit Board
PDU	Power Distribution Unit
PWM	Pulse Width Modulation
R	Resistance
RS	Recommended Standard
SH	Sensor Head
SPI	Serial Peripheral Interface
SU	Sensor Unit
T	Teslas
TLL	Transistor-Transistor Logic
TTI	Tecnologías de Telecomunicaciones e Información
TVT	Thermal Vacuum Test
UPM	Universidad Politécnica Madrid
USART	Universal Synchronous and Asynchronous Receiver-Transmitter
uC	microcontroller
UT	University of Trier
V	volts
VSM	Vibrating Sample Magnetometer

1. INTRODUCTION

NEWTON project targets to provide a fist opportunity to perform high resolution and complete non-invasive in-situ magnetic characterization of planetary surfaces and subsurfaces by means of developing a new portable and compact multi-sensor instrument which combines complex susceptibility and vector measurements. This instrument includes a magnetometer, a novel portable susceptometer, a power supply system and an electronic control with a frequency generation system.

The combination of magnetometers and susceptometers gives relevant information about the rocks composition, the history and the evolution of the planetary magnetic fields. This data will contribute to open a new via in the understanding of key questions related to the Solar System exploration which are still open. Questions as the intense magnetic anomalies of Mars, the characteristics of its past field, the origin of its moons, i.e. Phobos and Deimos, or even whether comets brought the life to the Earth can find some answers with the new data provided by NEWTON instrument. In addition to this, NEWTON provides also advantages in non-space technology fields among the ones it could be highlighted the application in civil engineering, in particular in the construction industry. NEWTON technology can be used for the soil, sediment and rock characterization in geotechnical works, the characterization of constructions materials such as concrete and bricks, to the detection of contamination soils and soft rocks with metals and the presence of cobalt and other contaminants particles in the concrete. With this regard, NEWTON instrument delivers better measurements interpretation which allows to reduce the time and cost of the prospections.

As already mentioned, with the aim of maximizing the impact of novel NEWTON technology, three different prototypes are being developed within the project. The prototypes which share the same architecture and provide different performance capabilities adapted to different scenarios are:

- **Prototype 1:** This prototype is designed for planetary exploration missions with the particular case of Martian and Moon's system with an envelope adapted to a rover-mounted payload. This prototype performs in-situ measurements of the complex susceptibility in a planetary environment combined with vector Natural Remanent Magnetization (NRM) data.

- **Prototype 2:** This prototype is a reduced version of prototype 1 implemented on a hand-held device for a rapid and preliminary analysis of surface during prospections on Earth. This prototype performs in-situ measurements of the susceptibility at discrete frequencies. It will be employed to potentiate the impact of NEWTON technology not only in space sector, but also on Earth for civil engineering applications.

- **Prototype 3:** This prototype is an advanced system for the in-situ analysis and full magnetic characterization of drilled samples in the medium term missions with more powerful rovers or to be part of base stations with the particular case of Martian and Moon's systems. This prototype performs in-situ measurement of the susceptibility, demagnetization and isothermal remanent magnetization (IRM) acquisition experiments.

This document describes the final design of NEWTON instrument prototype 3. The final design of NEWTON instrument prototype 1 and 2 are respectively reported in deliverables D3.4 [1] and D3.5 [2].

2. NEWTON PROTOTYPE 3

The block diagram of the NEWTON multi-sensor instrument prototype 3 is illustrated in FIGURE 1. As it can be seen in the figure, the instrument is integrated by three key building blocks, i.e. the Sensor Unit (SU), the electronic Control Unit (CU) and the Power Distribution Unit (PDU). At the same time, the SU is divided into the sensor head, which includes magnetometer and susceptometer, and the proximity electronics.

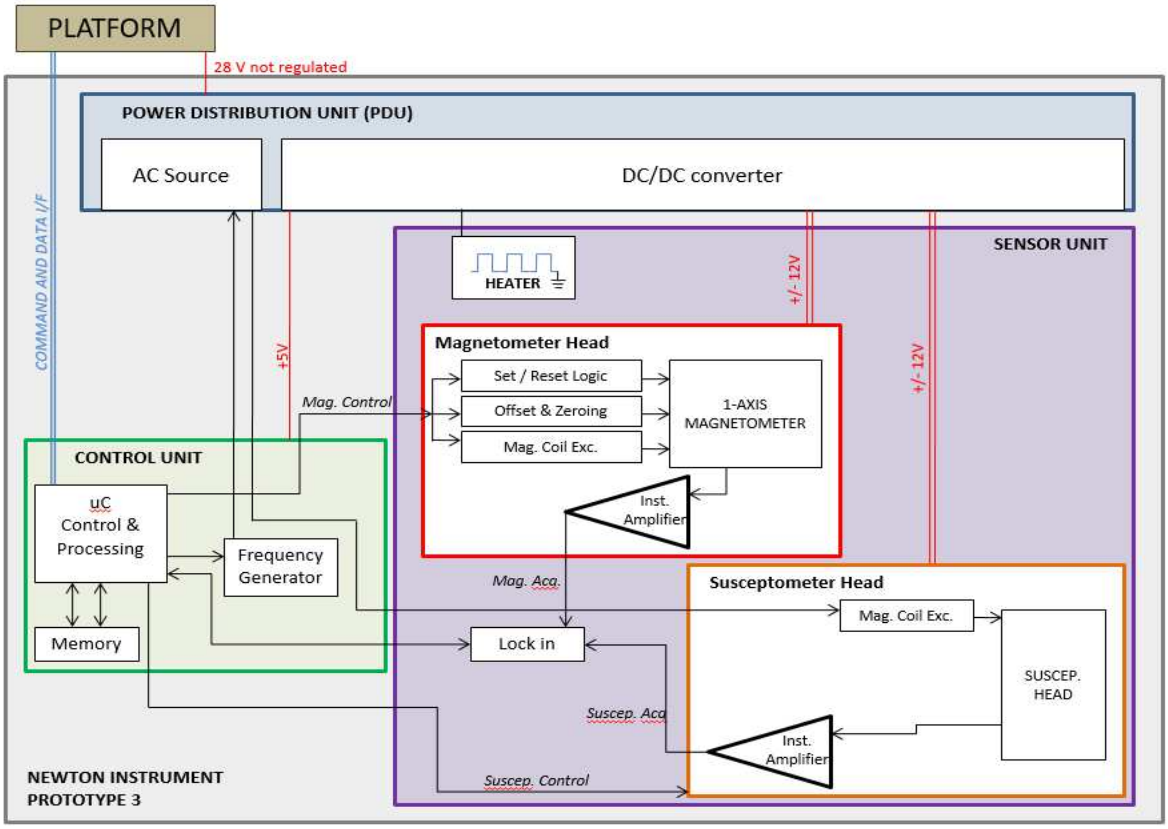

FIGURE 1. Block Diagram of the NEWTON multi-sensor instrument for prototype 3.

The Sensor Unit

The Sensor Unit is designed to perform the measurement of the susceptibility, demagnetization and isothermal remanent magnetization (IRM) acquisition experiments. For this purpose, the sample must be placed directly on the sensor head. The measurements will include:

a) a stepwise demagnetization of the Natural Remanent Magnetization by alternating fields,

b) minor hysteresis loops and

c) Isothermal Remanent Magnetization

The magnetometer will measure the remanent magnetization at several steps of magnetization / demagnetization processes. Together with the NRM data, these data allow to constrain paleofield strengths during formation of different minerals when they cooled below distinct transition (Curie/Néel) temperatures. This device is also thought to be very useful in applied geology.

The prototype is based on two designs for different range of frequencies. First , for 1 kHz up to 100 kHz and the second one for very low frequencies.

The prototype 3 first device performs magnetic flux measurements to characterize the magnetic properties of the materials. This kind of measurements is not frequency dependant, and has very good sensitivity. The sample is moved by means of a linear actuator within a secondary (pick up) coil system which measures the flux changes produced by the presence of an alternating magnetic field set by a primary coil. Such flux changes can be due either by changes in the sample magnetization or by displacing of the sample in the coil system. Performing a double Lock-in analysis at the frequency of the linear actuator and at the frequency of the applied magnetic field respectively, the signal from the pick-up coil provides the information needed for the analysis of the magnetic properties of the sample.

The second device of prototype 3 is a DC-ultra low frequency intense magnetic field production system. Some proposed magnetic measurements require low frequencies and strong magnetic fields. This device is based on a mechanical vibrating system, which limits the working frequency, and a big electromagnet to achieve the high field. A set of pick-up coils are used to collect the magnetization state of the sample under test. The working principles are similar to those of the first device, but with the main difference that in this case the applied magnetic field is a DC field and the frequency is that of the mechanical vibrating system, allowing the high magnetic fields previously mentioned but limiting the upper frequencies from an ultra-low to low frequency range.

The system will be used to perform measurements of samples commonly used in prospections by geologists. Sample geometry uses to be cylindrical with typical dimensions around 2 cm diameter and 2 cm length. The expected measurements are foreseen at low frequency susceptibility (DC – 1 KHz), magnetization curves (DC-1KHz) and high frequency susceptibility (1 KHz – 100 KHz).

The Power Distribution Unit

As in prototype 1 and 2, the PDU is integrated by the DC/DC converter and the AC current source. On one hand, the DC/DC converter is the same as in prototype 1 [1]. On the other hand, the demand of AC current of prototype 3 needs an ad hoc development. Therefore, an AC current source has been designed for the prototype 3, based on a full bridge switching, as it is described in section 5.

The Control Unit

The Control Unit (CU) main part is a microcontroller. This unit is divided physically for optimization and in order to improve the signal to noise ratio between the CU and the SU. Apart from the micro controller, the CU includes an oscillator to generate a stable reference frequency and a memory to save the input data measurements. The lock-in amplifier is allocated inside the SU module to be able to perform an analog lock in. A Digital Signal Processing (DSP) lock in was studied but it was discarded due to the extra complexity added regarding the speed of sampling related to the measuring frequencies (DC to 100 kHz).

The Electronic Control Unit is the responsible of the control, acquisition and processing of the signals of the sensor unit. The microcontroller performs these tasks as well as generates the different frequency signals for the susceptometer and magnetometer.

Interface

As in the case of prototype 1 and 2, the instrument has two electrical interfaces with the platform for communication and power supply purposes. The communication interface will be emulated by a PC. Regarding the power interface, prototype 3 will be validated in the laboratory and in principle it is not expected to test this equipment on field campaigns, therefore a laboratory power source will be used as the power interface with the platform.

3. SENSOR UNIT

3.1. Overview and target requirements

The NEWTON instrument prototype 3 will be used to perform measurements of samples commonly used in prospections by geologists. Sample geometry is usually cylindrical with typical dimensions around 2 cm diameter and 2 cm length. The expected measurements are low frequency susceptibility (DC- 1KHz), magnetization curves (DC-1KHz) and high frequency susceptibility (1KHz-100KHz).

To perform low frequency susceptibility and magnetization curves a Vibrating Sample Magnetization, VSM, system is commonly used. However, the sample weight and the portability of the system prevent its use for the present purpose. Another option is to perform magnetic flux measurements. This kind of measurements is not frequency dependant, and has enough sensitivity. Basically, these measurements are based on placing the sample in a coil system and to measure the flux changes produced in the coils. Such flux changes can be due either by changes in the sample magnetization or by displacement of the sample in the coil system. The flux changes are measured by integrating the induced electromotive force generated in the coils with an electronic integrator.

The mass susceptibility measurements, χ_m are intrinsically difficult because of the wide range of their possible values. It is also important to take into account the demagnetizing factor of the samples. The magnetization, M, of a sample with mass susceptibility χ_m, under the action of an applied field, H is given by:

$$M = \chi v \cdot (H - N \cdot (M - H)) \tag{3.1-1}$$

where N is the demagnetizing factor. Being $\chi_v = \chi_m \rho$, (ρ is the density), the volume susceptibility, it is easy to show that the effective volume susceptibility, χ_{ve}, is:

$$\chi ve = \frac{\chi m \rho (N+1)}{\chi m N \rho + 1} \tag{3.1-2}$$

In our experimental set up we will measure the change in the magnetic flux produced when the sample is magnetized for an H field that goes from 0 to H. For a cylindrical sample with diameter d and length h, the flux Φ_c induced in an n turns coil placed around the sample is:

$$\Phi c := \mu o \cdot (M - N \cdot (M - H)) \cdot \left(\frac{d}{2}\right)^2 \cdot \pi \cdot n - \mu o \cdot \mathrm{H} \cdot \left(\frac{d}{2}\right)^2 \cdot \pi \cdot n \tag{3.1-3}$$

or:

$$\Phi c = \frac{1}{4} \mu o \left(\frac{\chi m \rho H (N+1)}{\chi m N \rho + 1} - N \left(\frac{\chi m \rho H (N+1)}{\chi m N \rho + 1} - H \right) \right) d^2 \pi n - \frac{1}{4} \mu o H d^2 \pi n \tag{3.1-4}$$

FIGURE 2 shows the calculated magnetic flux Φc induced in a n=100 turns coil by a cylindrical sample with diameter d=2 cm, length l=2 cm, demagnetizing factor N=0.27, density ρ=5000 kg/m^3 and an applied field H=8000 A/m.

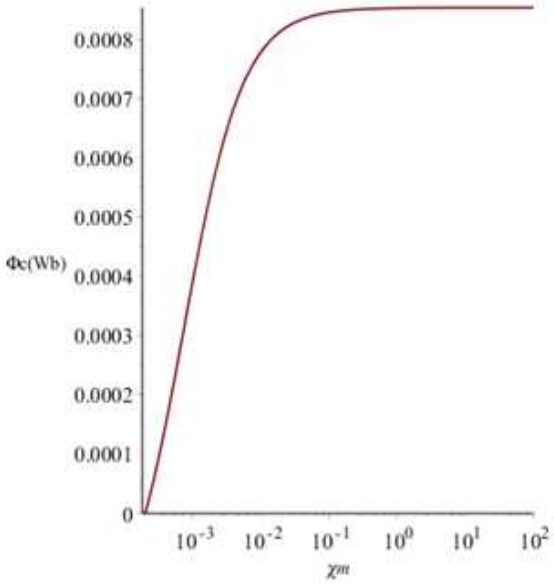

FIGURE 2. Magnetic flux produced by primary coil.

It can be observed that the magnetic flux is almost constant for mass susceptibility over 10^{-1}. To perform measurements over these values it is then necessary to change the shape of the sample in order to reduce the demagnetizing factor.

FIGURE 3 shows the same curve for a sample with a diameter of 0.2 cm and a demagnetizing factor of 0.017. It can be conclided that the system resolution must be in the order of 10^{-6} T m^2.

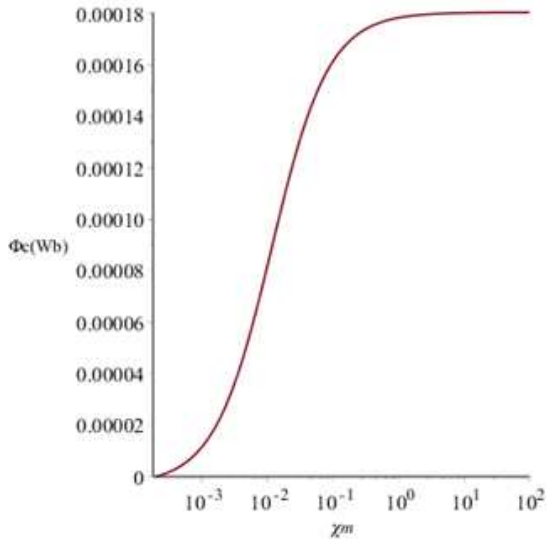

FIGURE 3. Magnetic flux with demagnetizing factor.

The dynamic range of the system must go from 0 up to the maximum expected value. To evaluate the maximum expected magnetic flux we have calculated the flux induced in a 100 turns coil by a cylinder of iron with the size mentioned above.

$$\Phi c := \frac{d}{2}^2 \pi n \cdot Ms \cdot (1 - N) = 0.046\, Tm^2 \qquad (3.1\text{-}5)$$

3.2. Detailed design

Measurements must be very accurate and for low susceptibility or magnetization measurements since the EMF induced by the field H can be orders of magnitude greater than the one induced by the sample. To avoid this part of the induced EMF in the secondary coil, the field H must be compensated. This compensation can be done with a second coil connected in opposition with the first coil and subject to the same field H, then it is necessary a very uniform H to guarantee that the both secondary coils are immersed in the same field. Additionally, both coils must be exactly equal in size, self-inductance and winding, which is almost impossible.

If the field H were not uniform, the compensation will be obtained displacing adequately the two coils, but we need a uniform field H to magnetize correctly the sample. We have solved the problem with a second pair of coils with less turns placed close to the end coils that produces the field H, this is in the zone were the magnetic field H changes abruptly.

There are three possible measurement modes:

1. To place the sample inside one central secondary and to change the field H to induce a magnetic flux change in the coils.
2. The sample is displaced alternatively from a coil to the other under a constant field H, in this case the flux change is only due to sample constant magnetization.
3. The sample is displaced alternatively from a coil to the other under an AC field H of constant amplitude. In this case the change in amplitude and phase of the AC induced EMF is only due to the sample alternating magnetization.

In 1 and 2 methods a fluxmeter integrator is used. In the third method a lock-in amplifier (section 4 in reference [1]) is used to measure the real and complex part of the susceptibility.

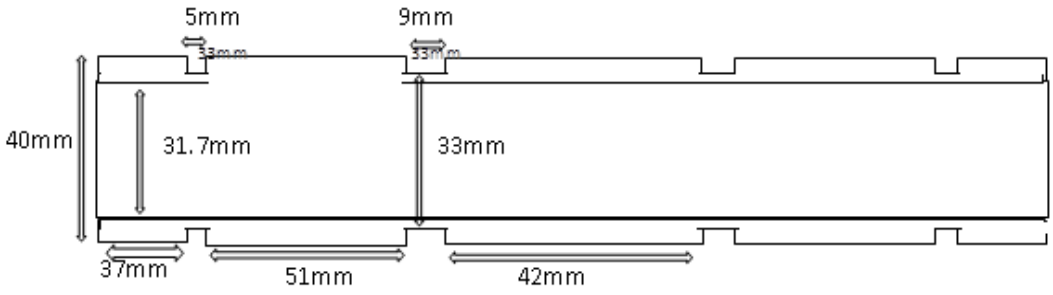

FIGURE 4. Prototype 3 secondary coil mould.

The sample holder diameter is given by the sample diameter and the secondary diameter is given by the sample holder diameter. Besides, the sample holder must displace inside secondary without mechanical contact to avoid spurious flux changes. Taking into account these conditions the dimensions of the secondary coil are shown in FIGURE 4. The signal induced in the secondary by the sample will depend on

the position inside the coil. With this regard, FIGURE5 shows the module of induced EMF by a calibrated coil *vs* position. The calibrated coils simulate a sample magnetized by an AC magnetic field.

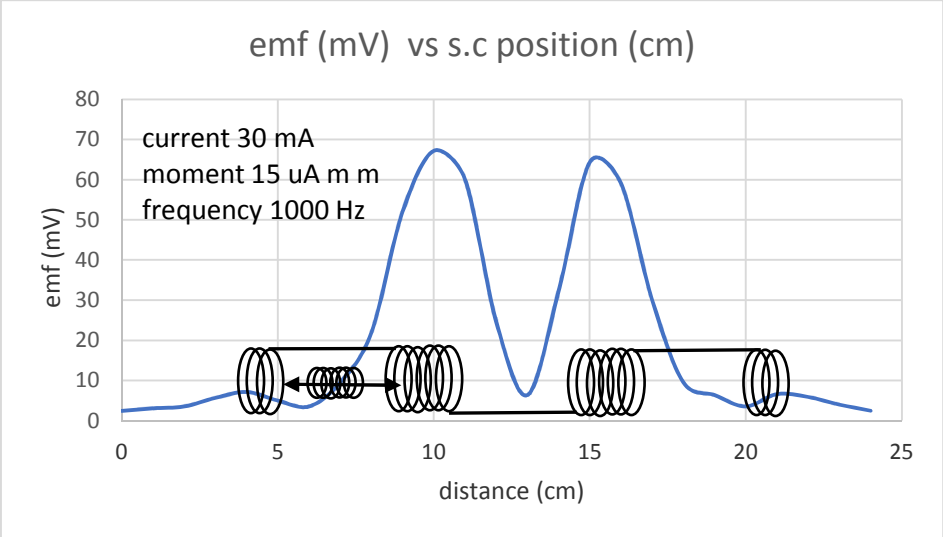

FIGURE 5. EMF vs sample position.

The head sensitivity is given by the number of turns, n, of the secondaries. The self-induction depends on n^2 so a trade-off between sensitivity and the self-induction needs to be achieved, as we will see later in the electronic design block. For the final system we propose several secondary heads depending on the working frequency. For this preliminary design we have selected 500 turns in central coils and 30 turns in the ends coils. The self-induction of this coil is 4 mH and a sample of $2 \cdot 10^{-4}$ mass susceptibility, a density of 5000 under a field of 80 A/m will induce e magnetic flux of 10^{-6} Wb. FIGURE 6 shows the behaviour of the secondary coil with frequency. The self-induction is 9.96 mH with a resistance of 30 Ω. It does not show any appreciable spurious capacitance. The secondary diameter is larger than any sample size, therefore, part of the flux produced by the sample will be lost. For this reason, a calibration is needed before any measurement as described in section 3.3.2.

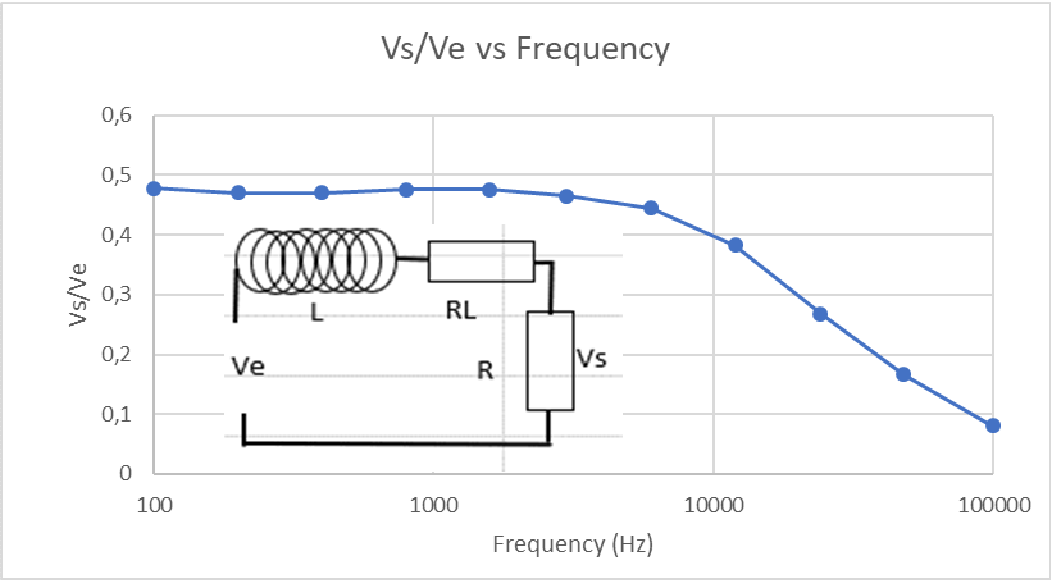

FIGURE 6. Behaviour of Secondary coil with frequency.

Primary Coil

For low frequency measurement, we will use the composed primary coil already presented in the previous report D3.2 [3] as shown in FIGURE 7:

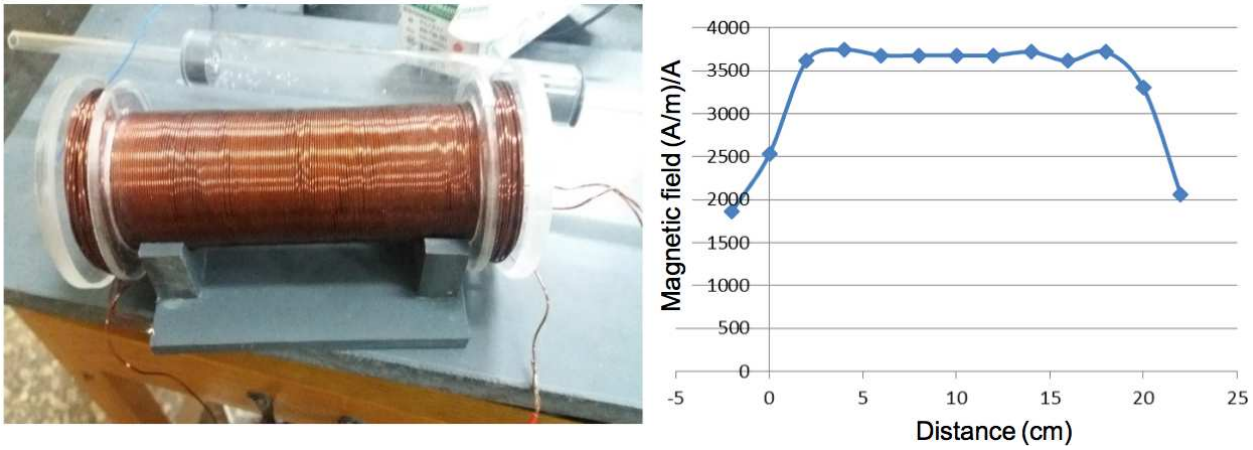

FIGURE 7. Magnetic coil for low frequency measurements.

The dimensions and feature of the magnetic coil are:

- 1 mm diameter wire.
- 4 layer in coil
- Resistance 4.7 Ohm
- Inductance 13.2 mH
- H field 3680 (A/m)/A
- The magnetic field uniformity in the central zone is about 1%.

To study the frequency behaviour of the coil in order to determine its frequency working range, we have used a searching coil shown in FIGURE 8 (0.1 mm wire diameter, 25mm coil diameter, 24.6 length, single layer of 216 turns).

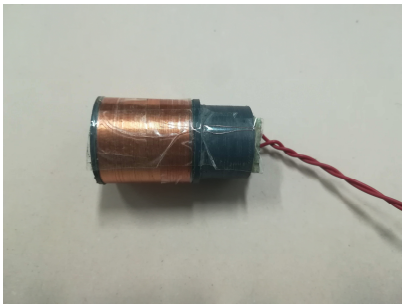

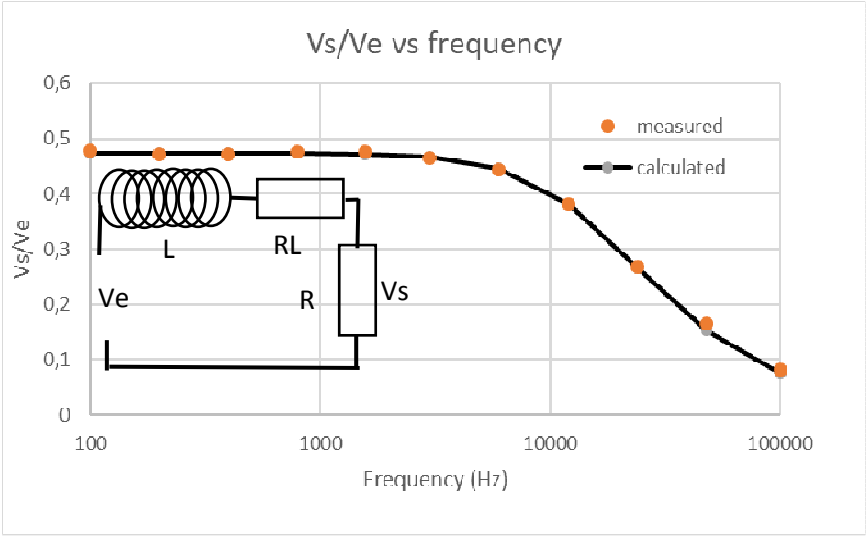

FIGURE 8. Searching coil to study solenoid frequency behavior.

A common source of error in this kind of research is the spurious capacitive interaction between turns. To reduce this error a single coil layer has been used. FIGURE 8 (right) shows the response with frequency of the searching coil assuming a self-induction of 738 µH and a resistance of 40.32 Ω. The calculated curve fits perfectly the measured one so the spurious capacitive is negligible.

FIGURE 9 shows the measured H field in the centre of the composed coil vs frequency. For frequencies over 20 KHz the measured field increases widely. In FIGURE 10 the current for a constant input voltage vs frequency is shown. It behaves as a resonant circuit due to the capacitive coupling between turns; therefore this coil can only be used for frequencies lower than 20 KHz.

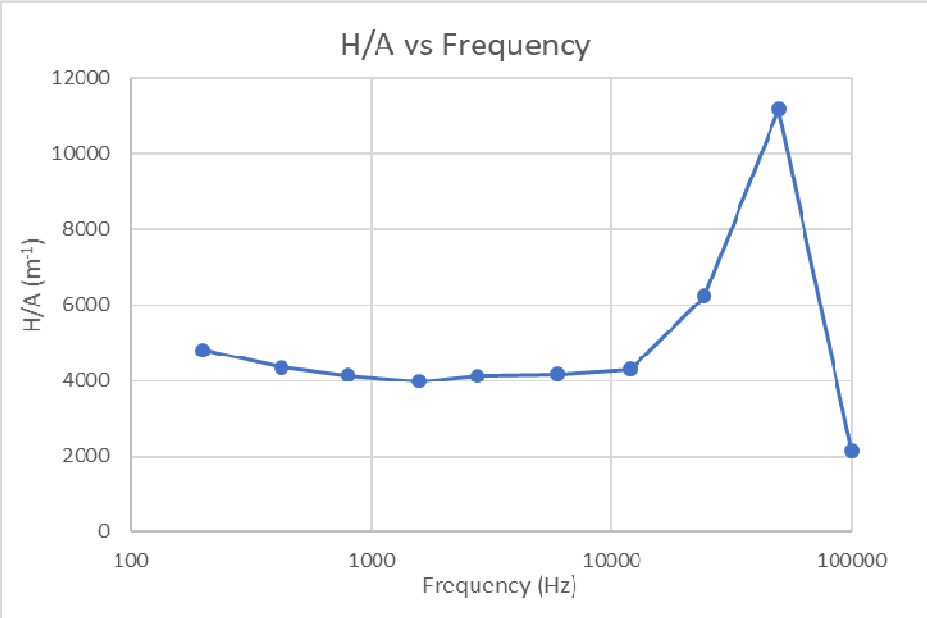

FIGURE 9. H field vs frequency. Over 20 KHz there is a non-measured extra-current due to resonance effects.

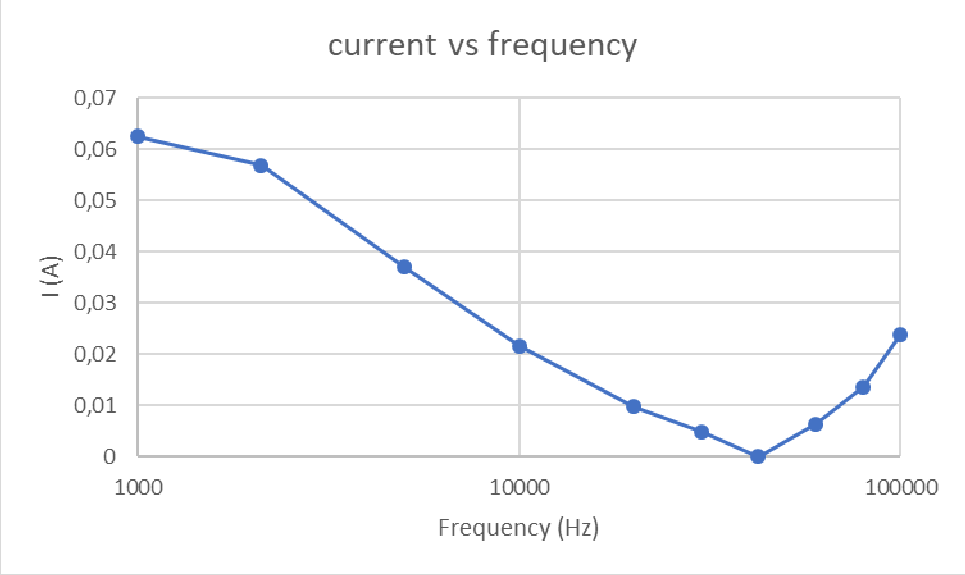

FIGURE 10. Current vs frequency. For frequencies larger than 20 KHz due to the capacitive coupling between turns, it behaves as a resonant circuit.

For higher frequencies a new set of coils has been designed. Such coils have only one layer-turn to reduce spurious capacitive effects and Eddy currents. A single layer turns implies that it must drive very high current to achieve the desired magnetic field and also there is a loss of uniformity in the magnetic field distribution as FIGURE 11 shows.

FIGURE 11. Magnetic field distribution inside a single layer turn coil.

We have tested two kinds of coils:

1. Coil made of copper tube to cool down the temperature during the measurement.

2. Coil made of several isolated copper wire (*Litz-like*) to reduce the Eddy Currents. In our case there are two wires of one mm in each turn. For the used frequencies the current goes through the whole section for this diameter.

In principle, the first option seems to be better because cooling is easier, but at the same time, the coil needs approximately double of the current. Besides, there is a zone along the tube where the magnetic field is very intense and there is a dissipation of power due to Eddy currents induced in the coil by the AC magnetic field out of the tube axi . In addition, there is a strong capacitive effect between turns**.** Such single layer turn coil and the behaviour with frequency is shown in FIGURE 12

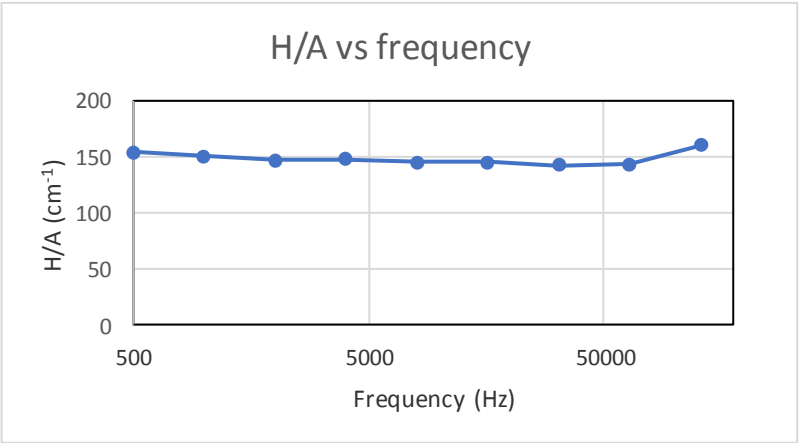

FIGURE 12. Single layer turn coil and its magnetic field behavior with frequency.

Regarding the second option, FIGURE 13 shows the coil made of several isolated copper wires (*Litz-like*). For the used frequencies the current goes through the whole section for this diameter. The perfect behaviour with frequency is shown as well.

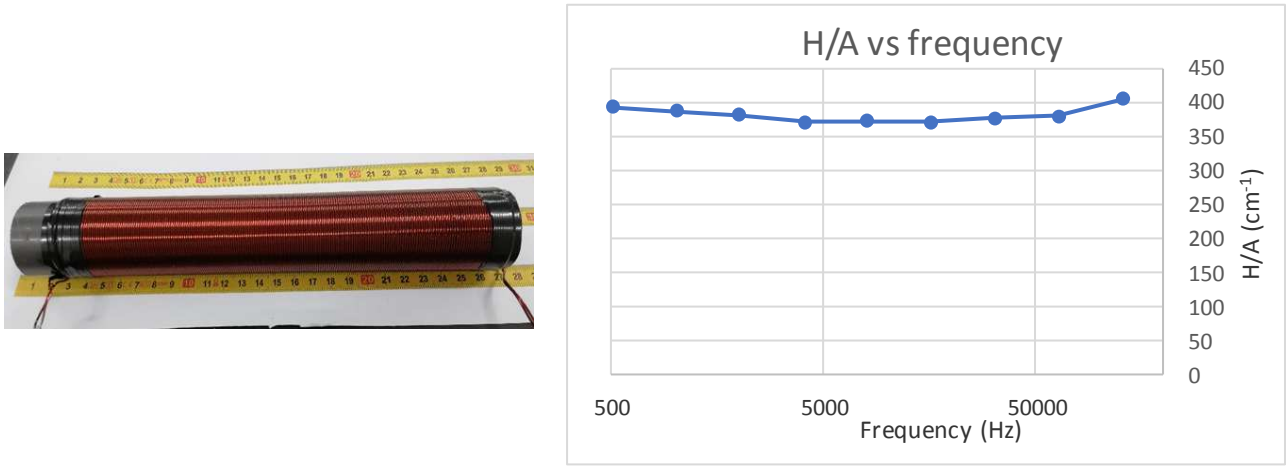

FIGURE 13. Coil made of several isolated copper wires. It is composed by two wires of one mm each turn (left). Magnetic field behavior with frequency (right).

As it can be seen by comparing FIGURES 12 and 13, the first option has worse frequency behaviour than the multi-wire one. However, the second option has an important problem regarding the proper cooling of the coil. To solve such a problem, a 3D printing has been used to build very thin walls tubes with a great rigidity that allow to refrigerate the coil by means of using a water flow inside of it. The design, the result of the tube and the final coiled plastic tube are shown in FIGURE 14.

FIGURE 14: Mechanical design to refrigerate the coil made of several isolated copper wires (upper figures). Lower figures show the prototype built up.

Second device: DC-ultra low frequency intense magnetic field production system

Magnetic measurements that require low frequencies and strong magnetic fields are commonly carried out using a Vibrating Sample Magnetometer (VSM). This device is based on a mechanical vibrating system, which limits the working frequency, and a big electromagnet to achieve the high field. Typical sample dimensions we may deal with (20 mm diameter, 20 mm length) cannot be measured in this kind of systems because of their relatively high weight (normally incompatible with the vibration system) and the size which exceeds the uniformity area of the magnetic field generated by the electromagnet (see FIGURE 16). For these samples, it would be necessary at least, 50 mm diameter poles to obtain an adequate uniformity in the zone of the gaps.

One possibility to solve the need of large magnetic poles is to change the poles shape in order to increase the field uniformity. Theoretically, a spherical cavity in a uniformly magnetized material will have a uniform magnetic field. However, due to the spherical symmetry, the demagnetizing factor will be 1/3. The maximum ideal magnetic field that could be reached into the cavity will therefore be 1/3 of the saturation magnetization of the material.

FIGURE 15 shows results from Finite Element Method (FEM) calculations on a ∅40mm spherical cavity into a pure iron ∅50mm rod with 220 mm length. As it is shown the uniformity along the axis and the perpendicular to the gap axis is very good. Maximum difference obtained in magnetic field B is about 1%. Magnetic field B into the rod is 1.2T, smaller than the saturation magnetization due to the demagnetizing field. The magnetic field into the cavity is 1/3 of the magnetic field in the solid region of the rod as expected.

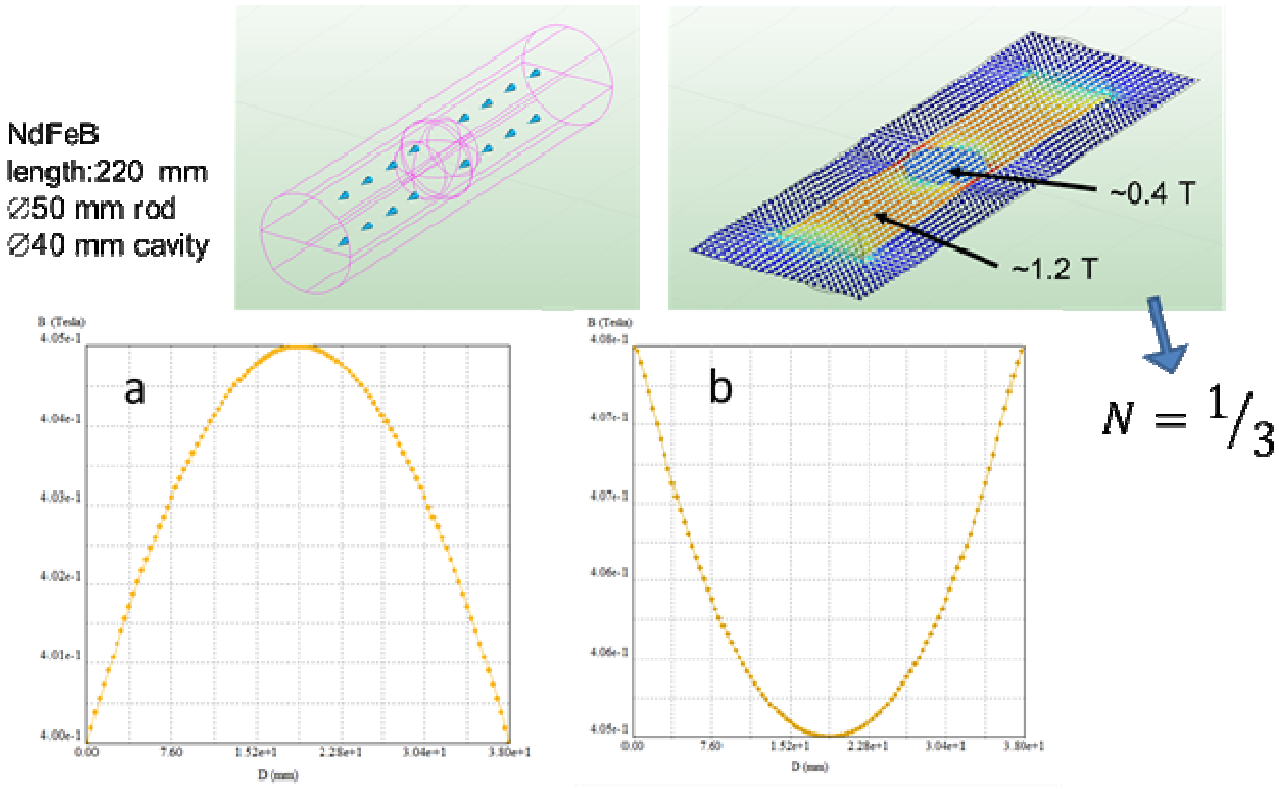

FIGURE 15: Simulation of magnetic field inside a spherical cavity. (a) Transversal. (b) Longitudinal.

In order to let the sample going into the spherical cavity a minimum gap spacing of 20mm is required. FIGURE 16 shows a spherical cavity in a pure iron ∅30mm pole diameter magnet designed with a 40mm diameter. This design has a spacing larger than 20mm thus allowing samples below these dimensions going into the uniform magnetic field region.

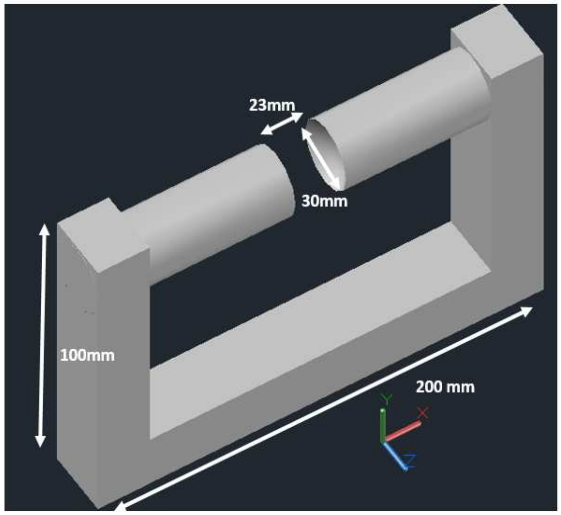

FIGURE 16. Single electromagnet.

The area of uniform field does not allow vibrating measurement. This can be solved by using two devices as shown in FIGURE 17.

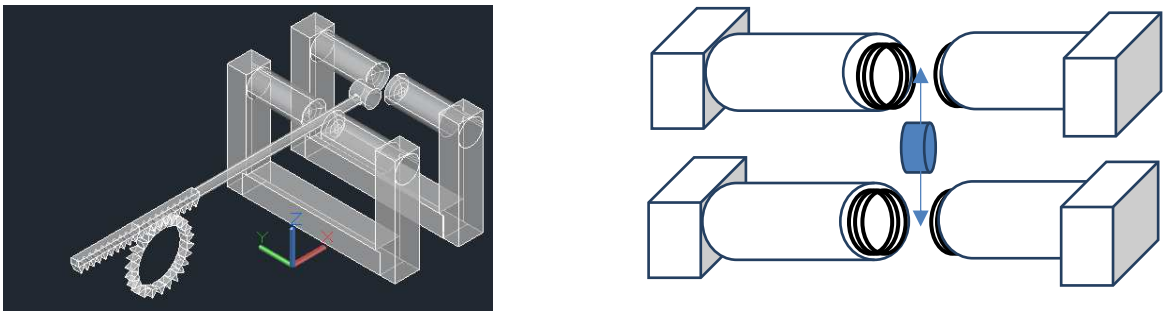

(A) (B)

FIGURE 17 (A): proposed configuration for the generation of the magnetic field. (B): detail of pick-up coils.

With this configuration we can perform two different kinds of magnetic measurements with the following procedures:

1. Sample magnetization measurement
   - Place two secondary coils in series in each electromagnet and connect both systems of secondary coils between them in series opposition.
   - Connect the electromagnet in series.
   - When the sample is displaced from an electromagnet to the other the change of the magnetic flux in the secondary coil system is due to sample magnetization.
2. Susceptibility and demagnetization measurements

- Place two secondary coils in series in each electromagnet and connect both systems of secondary coils between them in series.
- Connect the electromagnet in series opposition.
- When the sample is displaced from an electromagnet to the other the change of magnetic flux in secondary coil system is due to the change of magnetization of the sample under the action of the topological alternating magnetic field.
- In both cases flux changes due to current oscillation in electromagnets are auto compensated in the secondary coils.

To reduce the size and weight of the device we have finally decided to use rare-earth magnets instead of electromagnets and one single structure with two spherical gaps as FIGURE 18 illustrates.

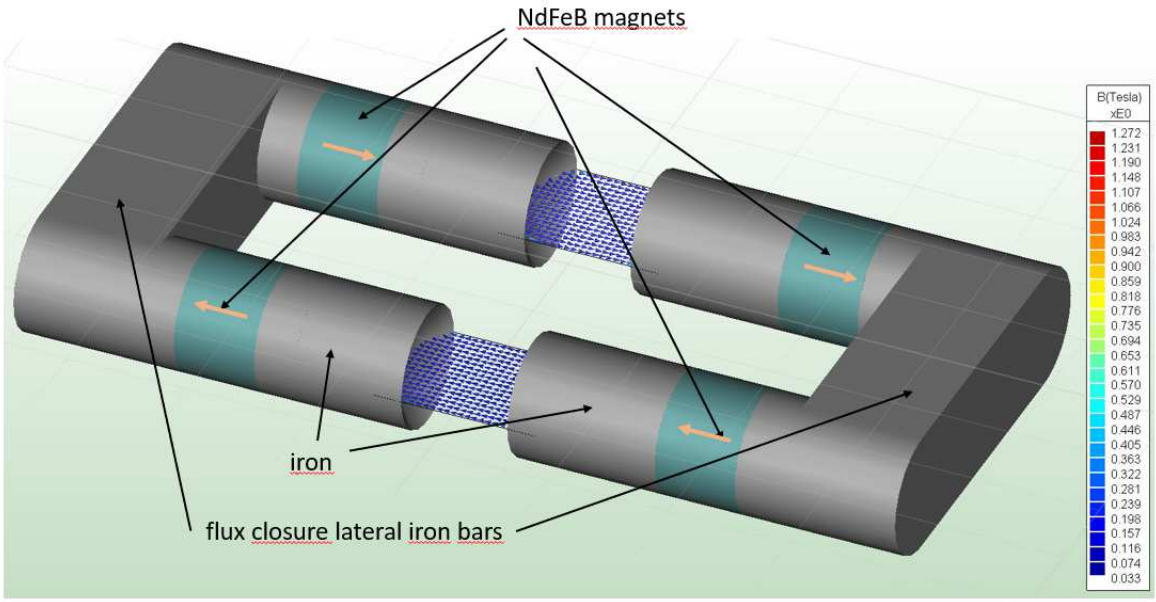

FIGURE 18 device with two pairs of magnets generating an antiparallel and uniform magnetic field in two spherical cavities.

The intensity of the magnetic field in the gap can be controlled by designing a support that allows modifying the distance between the magnets and the lateral iron bar used for flux closure. This mechanism avoids modifying the geometry of the gap and so maintaining the uniformity of the magnetic field while mechanically reducing the flux closure. The final prototype designed is shown in FIGURE 19.

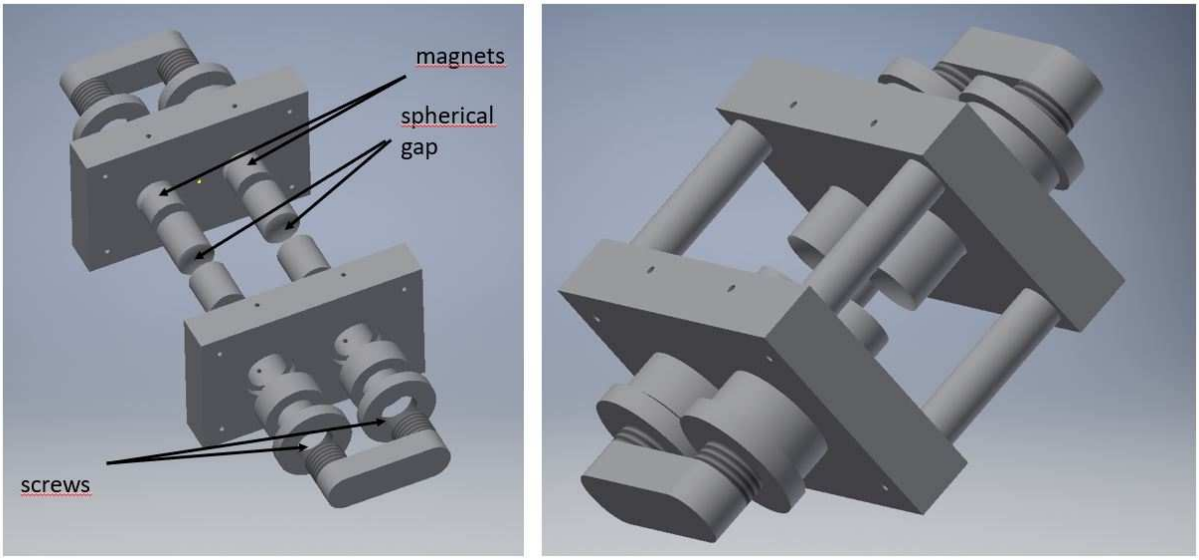

FIGURE 19 Mechanical design

We have evaluated the expected magnetic field achieved by FEM. Results are shown in FIGURE 20. The uniformity is reduced with respect to the one obtained for the complete spherical cavity shown in FIGURE15. This is due to the reduction of the cavity dimensions in order to open a lateral access larger than 20mm to allow sample access to the gap.

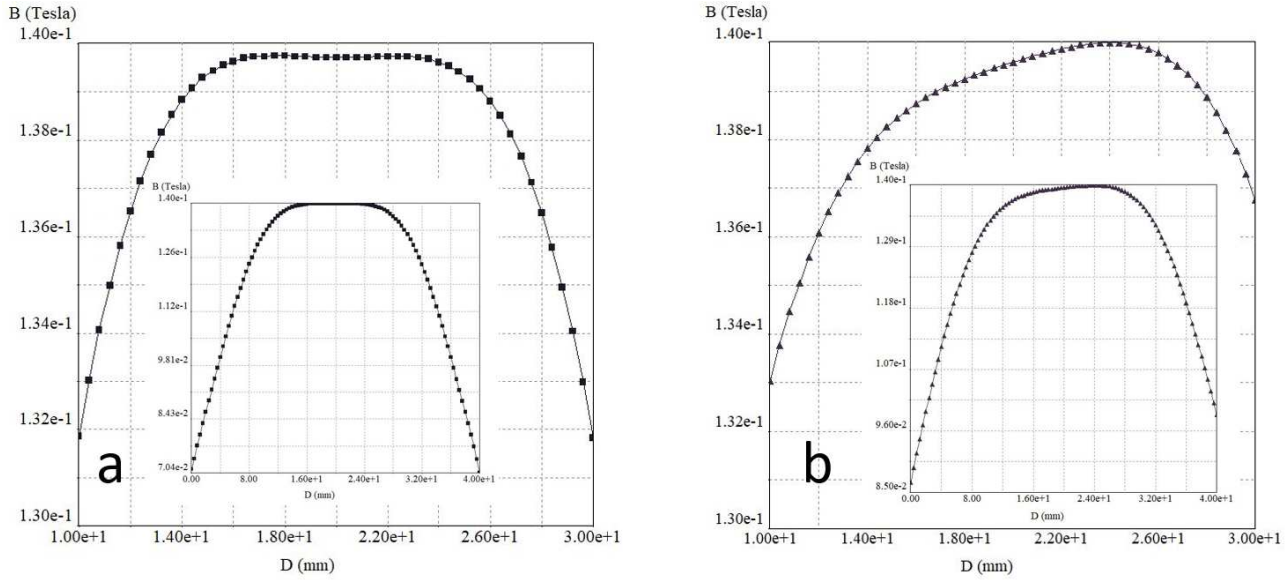

FIGURE 20: Magnetic field into the gap along the a) axis, and b) perpendicular to the axis. Main curves correspond to a length of 20mm while insets correspond to 40mm.

Figures 20 show the magnetic field along the axis in the center of the cavity for the maximum length that the sample can occupy (20mm). Changes in magnetic field B are smaller than a 6% along the longitudinal axis (a) and below 5% along the perpendicular to the axis (b). Insets show the magnetic field for a longer distance (40mm) and it is shown how the magnetic field is notably reduced. It will be required to place the sample in the gap center carefully to allow loss of uniformity. Fabricated prototype is shown in FIGURE 21. We have measured a magnetic field of 0.15T very close to that expected from FEM simulations on final

prototype. With this new configuration, the magnetic field only depends on the position of the lateral closure flux bars and on the magnets position (iron poles are fixed).

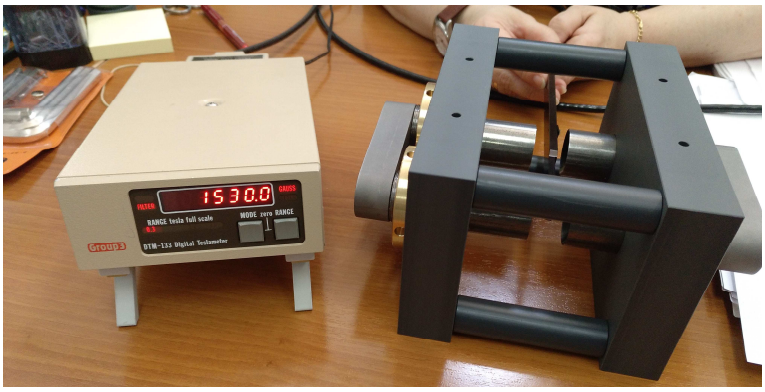

FIGURE 21: Magnetic field measurements on fabricated prototype for the magnetic field generation.

3.3. Manufacturing, Validation DATA and calibration

3.3.1. Manufacturing

FIGURE 22 shows the secondary set up with the four secondary coils to compensate EMF induced by H. Plastic screws are used to produce a micro displacement inside the primary coils

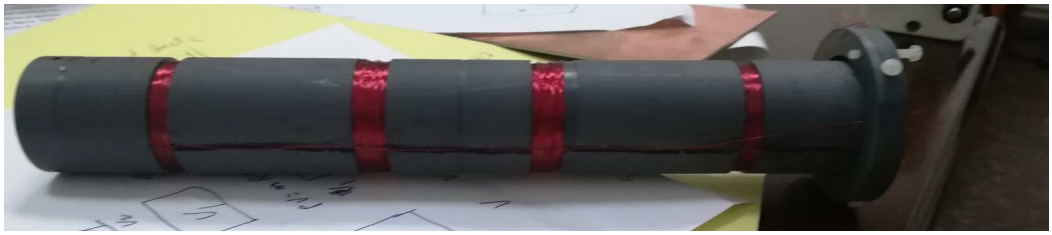

FIGURE 22. Secondary coil of prototype 3.

In FIGURE 23 the mechanical part of the experimental set up, i.e. the sample holder and the stepper motor displacement system it is shown. The sample holder is made of methacrylate for this laboratory set up and the length is the adequate to do not induce magnetic flux changes in secondary coils when it is displaced by the stepper motor. The distance between sample and stepper motor is large enough to avoid spurious inductions.

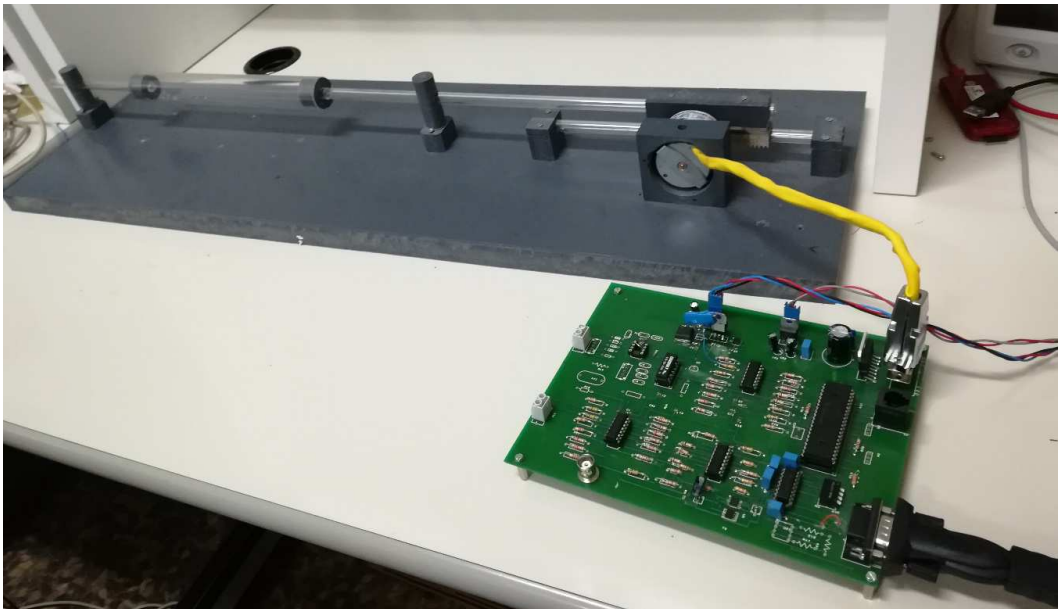

FIGURE 23. Linear actuator of prototype 3.

FIGURE 24 shows the whole experimental set up including the electronic circuit control board and the connection with the stepper motor. The diameter of the tube of the sample holder has been increased in order to allow the rotation of the sample inside. In this way, anisotropy measurement can be performed.

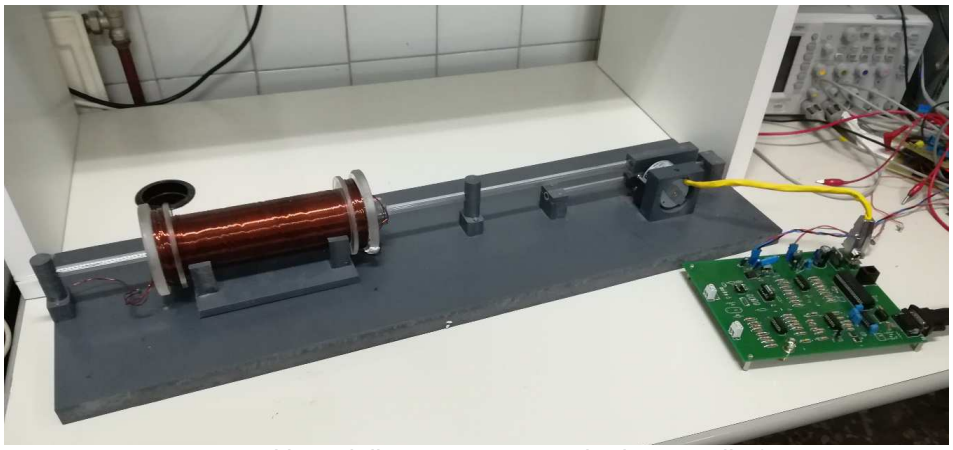

FIGURE 24. Control board, linear actuator and primary coil of prototype 3.

For high frequency measurements a primary coil with a single layer made of two wires of 1mm diameter, as it has been described before in FIGURE 14 is used. Regarding the previous design developed for the preliminary design, the heating problem has been solved by refrigerating the coil support.

Final measurements require the electronic unit integration. Up to now, we have tested and calibrated the coils for magnetic H production as well as the secondary coils. We have also tested the software and hardware related to:

1. The serial communications between the PC and the devices.
2. ADCs
    - Configuration: it allows the configuration of the microcontrollers ADC inputs selecting the actives and its voltages references.

- Single measure mode: the selected ADC performs a single measure and sends results to PC.
- Average measurement mode: the selected ADC performs *n* measurements during a selected time interval performing an average and sending results to PC.
- Multiple measurement mode: the selected ADC performs *m* averaged measurements during a selected time and after each averaged measurement sends the results to PC.

3. DACs
   - Voltage generators for drift and level control
   - Ramps generation and measurement system. It works adequately; it is able to generate ramps of 2^{13}-1 steps performing averaged measurements each *k* selected steps sending the results to PC.
4. Stepper motor control
   - It moves the motor a specified number of steps in a specified time interval and it is also able to create periodical displacement.
   - It can perform averaged measurements each *k* selected steps sending the results to PC.

The preliminary design of the electronic part has been redesigned to improve the offset and drift control. A memory has been included in the previous circuit to increase the speed in data acquisition. It will be described in Section 4 of this document.

3.3.2. Validation Data and Calibration

The main problem of this kind of measurement systems is the different diameter between the coils and the samples. This situation is very common in devices designed to measure magnetic samples by induction as is the case in Vibrating Sample Magnetometers. To overcome this problem a well-known sample is usually supplied for calibrating the induction in secondary coils. This calibration requires saturating the sample and so, a high magnetic field is needed. This saturation cannot be reached with a primary coil as that in our system so such kind of calibration is not appropriate. To overcome this problem we have found a simple solution. We have fabricated some cylinders as FIGURE25 illustrates (d=20 mm diameter, l_c=20 mm length, and d=25 mm diameter, l_c=25 mm length). We have also wound a copper wire to build a continuous coil with a well-known magnetic moment. A current of I amperes circulating through the N turns makes the coils behave like a magnetic sample with a magnetization:

$$M = \frac{IN}{l_c} \tag{3.3-1}$$

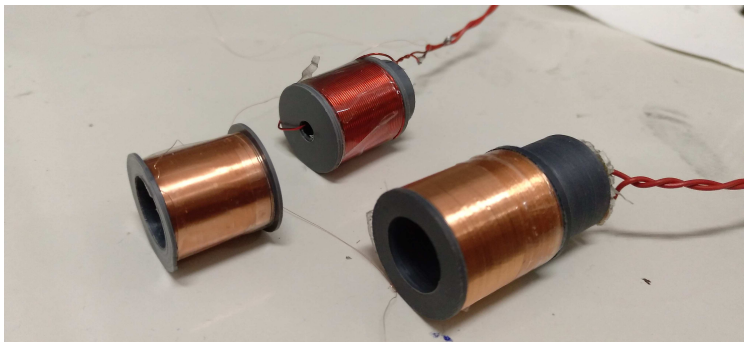

FIGURE 25. Example of coils to be used for calibration.

Fluxmeter calibration and test procedure:

1. An AC current of I amplitude is applied to the calibration coil.
2. The calibration coil is displaced inside the secondary connected to the fluxmeter integrator up to obtaining the maximum value of the induced EMF.
3. The calibration factor is $(I\ N/l_c)\ /V_f$, being V_f the voltage at the fluxmeter integrator output

FIGURE 26 shows the response of the system (chanel1: upper trace) versus current (chanel2 voltage/20Ω). For a 10000 turns/m calibrated coil used in this test, the calibration factor is 1.2 µT/mV. (A common commercial VSM minimum measure is 6 µT of magnetization in a volume of 100 mm^3). To obtain this sensitivity, a resistance of 1 KΩ as input the integrator and a capacitor of 56 nF as operational feedback have been used.

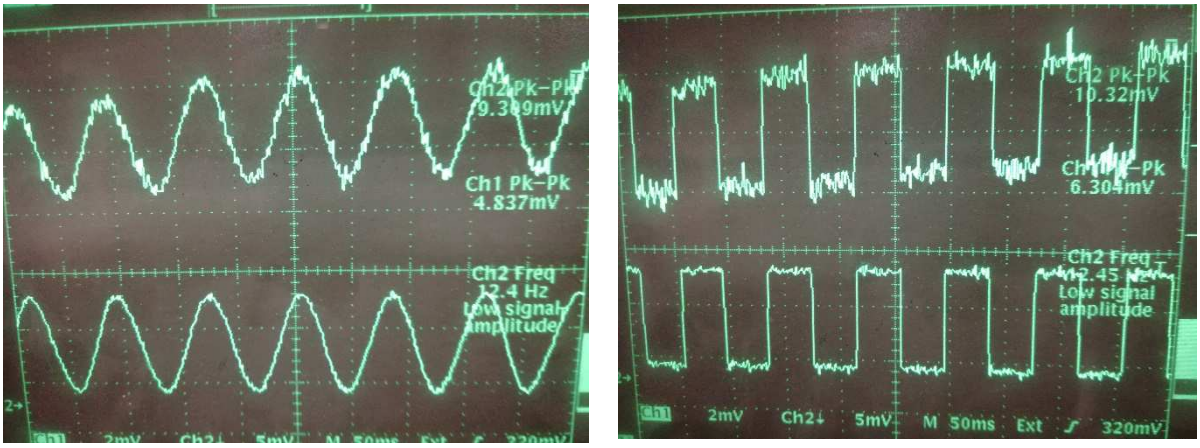

FIGURE 26. Response of the system vs current.

The linearity of the system can be observed in FIGURE 27. For frequencies over 150 Hz a phase due to the secondary Impedance (30 Ω, 9.6 mH, Lω= 10Ω) appears in the response of the system (FIGURE 27 right). The system does not work when the inductive impedance is higher than 1% of the input resistance.

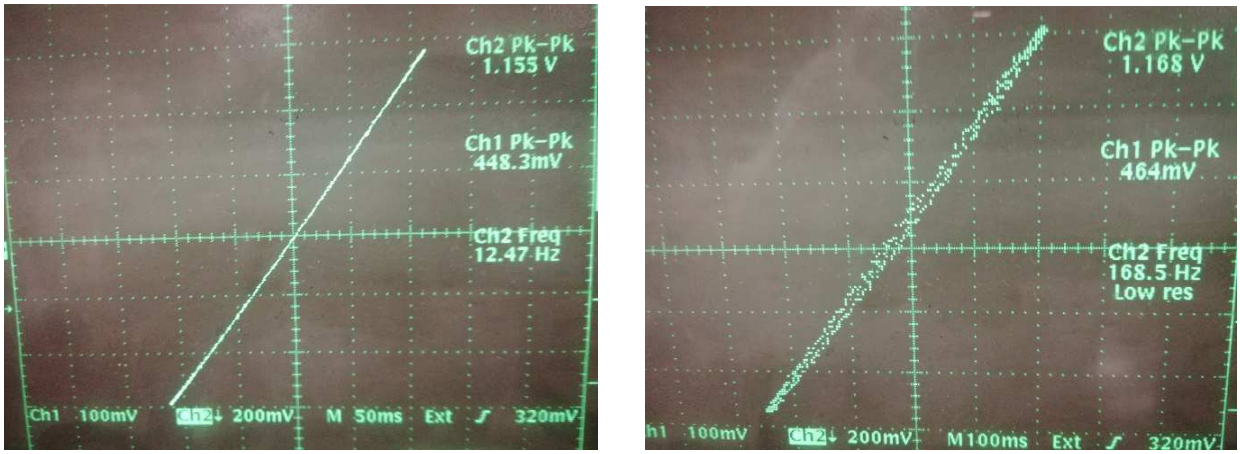

FIGURE 27: Response of the fluxmeter integrator for 1 KΩ of input resistance at the integrator and a capacitor of 56 nF.

For higher input resistances the sensitivity is reduced but the frequency range increases. In FIGURE 28 the input resistance is 17.4 KΩ at 3 KHz (left) the answer is perfectly linear and the phase effect appears at frequencies in the order of 30 KHz (right).

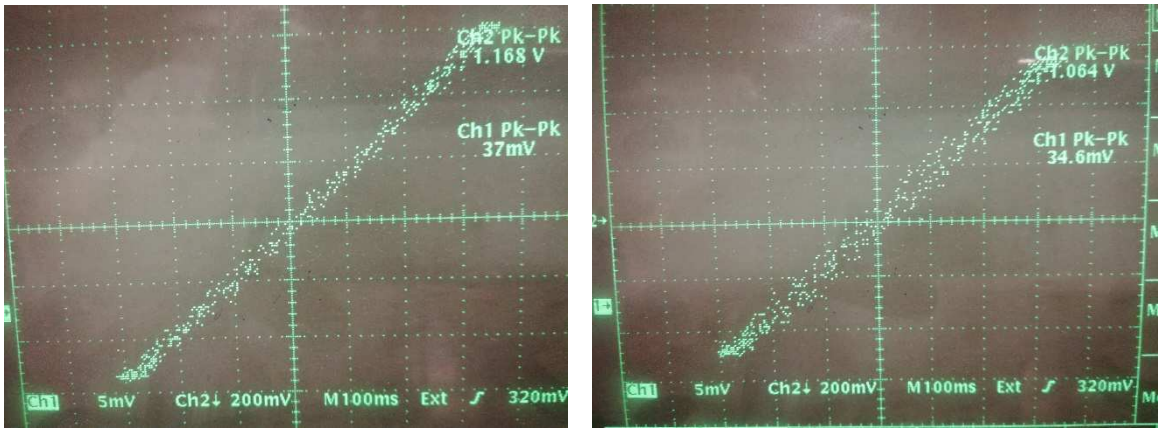

FIGURE 28: Response of the fluxmeter integrator for 17.4 KΩ at 3 KHz (left) and at 30 KHz (right).

To perform correct measurements:

- It is necessary to perform a calibration with the calibrating coil. The sensitivity will depend on the selected input resistance and capacitive feedback.
- The maximum working frequency is given by the secondary self-induction *L*. The product $L2\pi f$ must be lower than the 1% of the input resistance.

Susceptibility calibration and test:

For susceptibility measurements, the induced magnetization and its phase respect to the applied field must be determined. In principle to calibrate the system it is necessary a sample with well-known both susceptibility and energy loss per cycle. A copper rod is a good option, but the calculation of the energy loss per cycle is not straightforward and therefore this is a source of error. To solve this problem, we have used the calibrating coils short circuited with a resistance.

If the coil is under the action of an AC Ha magnetic field, the induced EMF in the calibrating coil is:

$$V_i = \mu_o N S \omega H_a \tag{3.3-2}$$

being *S* the coil section, *N* de number of turns and $\omega = 2\pi f$. The current in the coil will be:

$$I = \frac{V_i}{\sqrt{R^2 + (L\omega)^2}} \tag{3.3-3}$$

being *R* the resistance of the coil and $L\omega$ the resistance due to the self-induction *L* of the coil. The phase between the current and the induced EMF is given by:

$$\phi = \frac{L\omega}{R} \tag{3.3-4}$$

To calibrate the system we need to follow the next steps:

1. To apply an AC current, I_c through the calibrating coil.
2. The secondary must be connected to a lock-in amplifier synchronized with the current signal through the calibrating coil.
3. With applied field zero (that is primary coil circuit open) move the calibrating coil along the secondary axis. The calibrating coil must be led in the place where the induced EMF (V_{cs}) in the

secondary is maximum. Phase Difference between V_{cs} and I_c must be 90º and we can calculate the relation I_c/V_{cs}.

4. Disconnect the calibrating coil from the current source without changing its position. Applying a well-known AC field H_a , we measure the induced voltage in the calibrating coil, V_i, whose phase is 90º respect to the H_a field.
5. Short circuit the ends of the calibrating coil with a resistance. Measure the Amplitude and the phase of the induced EMF in the secondary. Those values must correspond to the calculated ones in equations (3.3-3) and (3.3-4).

Table 1 shows the measured current and phase for a calibrating coil frequency of 10850 Hz.

TABLE 1: Measured current and phase.

R (Ω)	CH1 (mV)	CH2 (mV)	Vi module	Phase
0	-56.2	74	92.9	-0.9
34.5	-54.5	38.5	66.7	-0.6
102	-36.8	14.2	39.4	-0.3
430	-12.25	2.15	12.4	-0.2
1018	-5.7	1.5	5.9	-0.3

TABLE 2: Calculated current and phase.

f (Hz)	*L* (H)	*L*ω (Ω)	$R+R_L$ (Ω)	Phase	V module (mV)
10890	7.35E-04	5.03E+01	4.11E+01	**1.22E+00**	92.2
10890	7.35E-04	5.03E+01	7.56E+01	6.65E-01	66.0
10890	7.35E-04	5.03E+01	1.43E+02	3.52E-01	39.5
10890	7.35E-04	5.03E+01	4.71E+02	1.07E-01	12.6
10890	7.35E-04	5.03E+01	1.06E+03	**4.75E-02**	5.6

As it can be seen in the TABLE 2, there are two values which deviate from theory. The first one corresponds to an external resistance of 0Ω. The real evaluation of such resistance is difficult because the unknown contact resistances become important. The last value corresponds to a resistance larger than the *L*ω value, and then the phase value is measured with a large error according to equation (3.3-4). We can obtain errors lower than 1% by characterizing the system calibrating coil resistance, by connecting it to a well-known AC voltage source.

4. ELECTRONIC CONTROL UNIT

4.1. Overview and target requirements

This section describes the advanced control functionality included in the Control Unit of the NEWTON prototype 3. This advanced system is dedicated to perform magnetic susceptibility measurements of samples in a portable system. There are two kinds of measurements: low frequency range and high frequency range. In this section we will describe the system able to perform the magnetic measurement and to generate the signal used to produce the exciting field. The signal generated in the secondary is proportional to the derivative of the magnetic flux, so it must be integrated to attain the magnetic flux and therefore the samples magnetization. To perform any magnetic measurement, changes in magnetic flux induced in the secondary coils must be produced. These changes can be done by varying the exciting field or by displacing the sample inside of the secondary coil system. In both cases the exciting field or sample position must be known or measured. In the following section both, the hardware and software of the whole device are described. An additional PCB will be used for the implementation of the advanced control system of the Prototype 3.

An analysis about susceptibility measurements requirements can be found in section 3.

4.2. Detailed Design

4.2.1. Electronic Circuit

FIGURE 29 shows the schematic of the electronic circuit designed for the prototype 3.

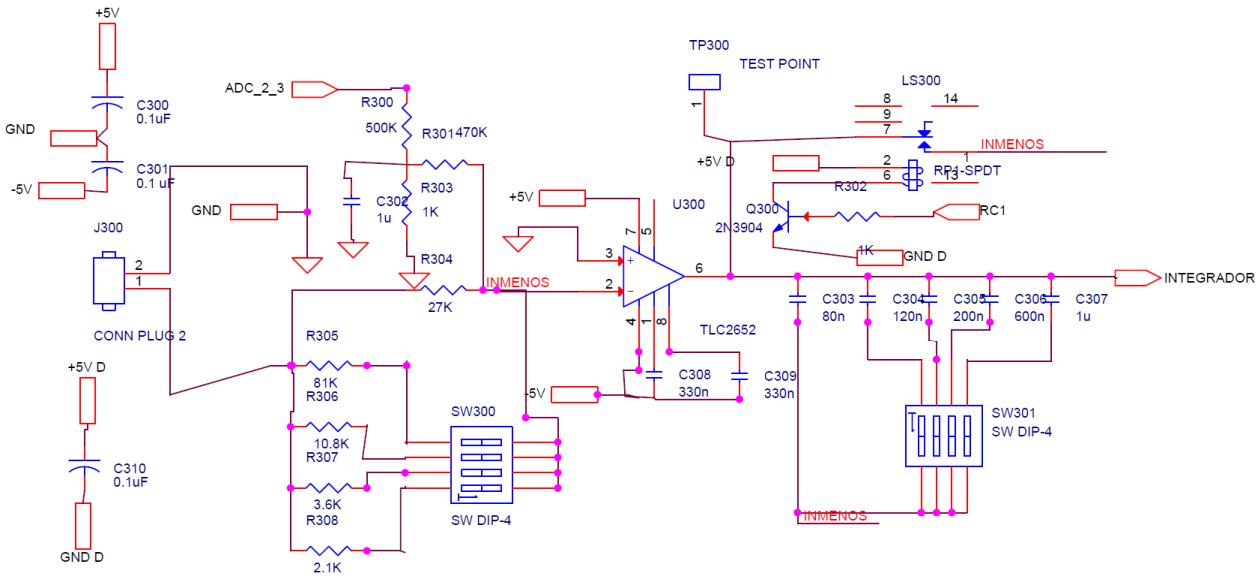

FIGURE 29. Schematic of the integrator prototype 3.

The integrator design is shown in the FIGURE 30**.** It is impossible to cover the measurement range with a single RC set in the integrator. So we will use a set of different resistances 1-270 KΩ and a set of high quality capacitors 0.01-3 µF. The output in the integrator is V= Φc/(RC), the maximum sensitivity will be 10^5 V/Wb and the minimum 10 V/Wb. This will be enough to cover the whole range. The sensitivity of the

whole system also depends on the number of turns of the secondary coil. In principle the coil geometry will always be the same and its self-induction can be evaluated, semi experimentally, as function of the number of coil turns. The self-induction of the secondary coil produces a spurious phase in the integrator that depends on the frequency. The signal from the integrator is amplified and displaced to allow its measure by de ADC of the microcontroller which allows to select by software the most adequate range. In addition to this, the offset level also can be controlled by software.

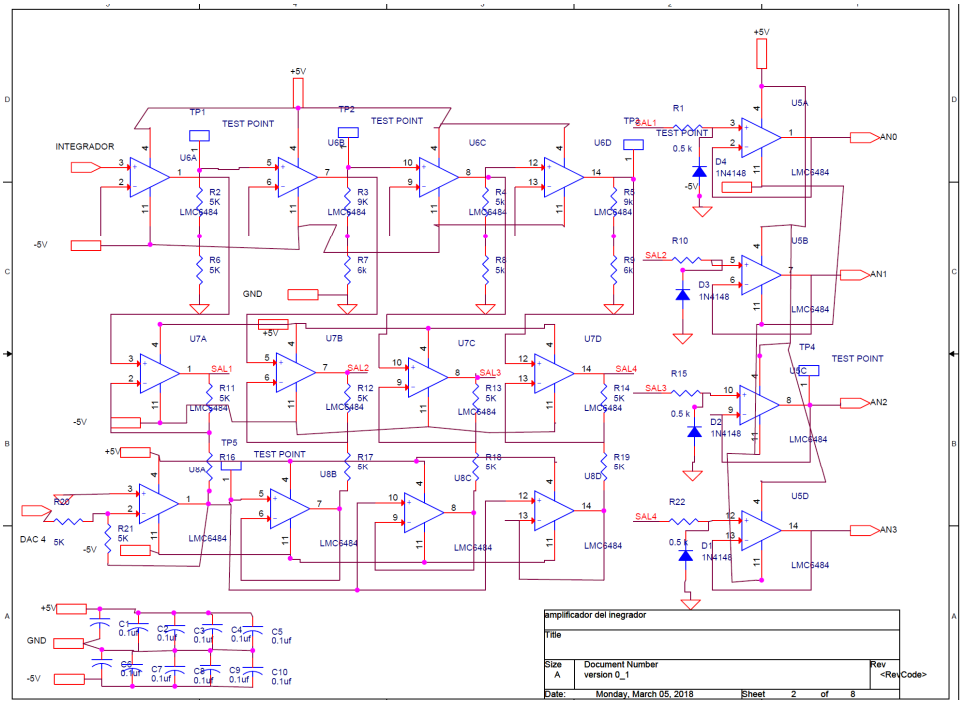

FIGURE 30. Schematic of the integrator signal conditioning and amplifiers.

FIGURE 31 shows the frequency vs the number of turns to have a phase lower than 10^{-3}. If we select an input resistance of 1 KΩ and 200 turns, the maximum working frequency is 100 Hz. The feedback capacitor is charged by the operational amplifier output and its current is limited to 40 mA, so large capacitors cannot be used at high frequency. FIGURE 32 shows the maximum capacitor which is allowed for each frequency.

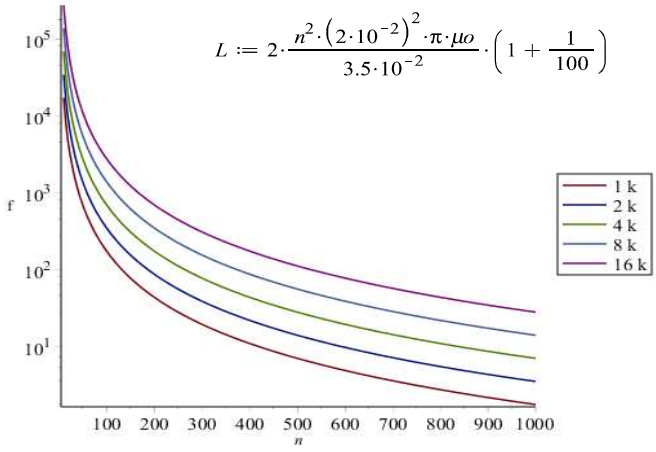

FIGURE 31. Frequency *vs* the number of turns.

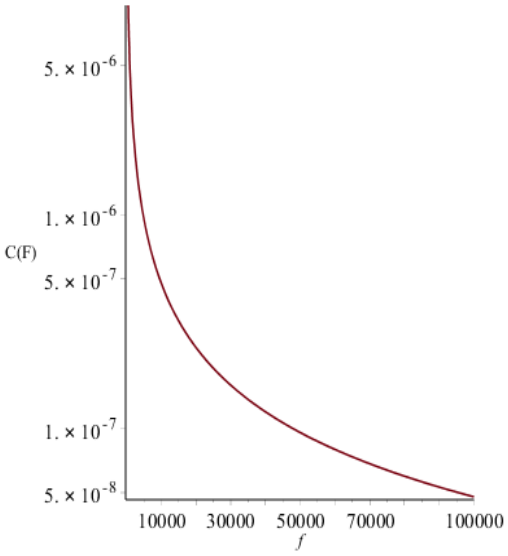

FIGURE 32. Maximum capacitor value allowed for each frequency.

To solve these problems, besides this manual adjustment of sensitivity, there is a chain of amplifiers connected to 4 ADCs of the µ-controller. This automatically adjusts the sensitivity range.

The main problem of the integrator is the drift because of the DC open loop. The sources of the drift are the Peltier voltage that appears in welded conductors and the current bias of the operational amplifier. We have been very careful with the conductor distribution looking for a symmetric configuration. Therefore we have also selected an appropriate operational amplifier. We can estimate an uncompensated drift current in the order of 100 pA so for 1 µF capacitor in the feedback, the output voltage drift is in the order of 10^{-4} V/s.

To compensate the thermal drift we have designed the input offset correction block consisting on two 10 bits DACs, connected to a differential amplifier to attain +/- 5V at the output. Tension divider and a capacitor are used to filter and stabilize the current used to compensate drift. After performing the drift compensation, the output can be out of the middle of the dynamic range so an offset tension supplied by another DAC is used to adjust the integrator output level at the correct voltage.

H field measurements:

To measure the field H we use a differential amplifier as input and 3 more amplifiers in cascade to obtain four different gain amplitudes. The offset level is controlled by 10 bits DAC (see FIGURE 33).

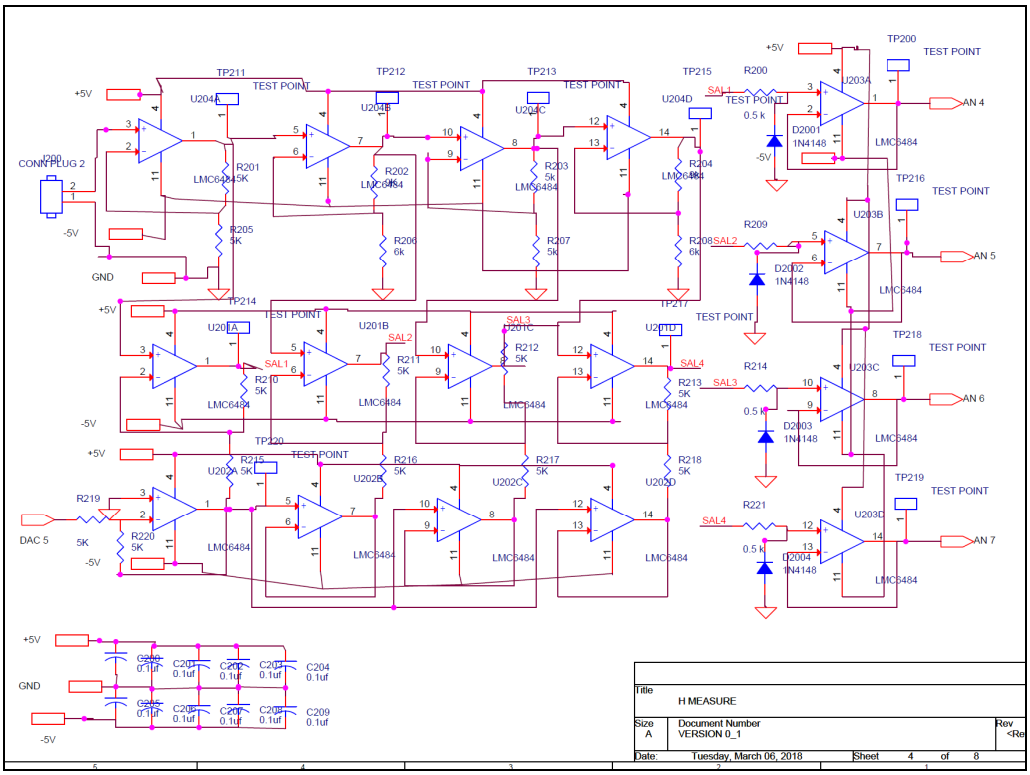

FIGURE 33. H field measurement circuit.

The H field is produced by a power amplifier controlled by the circuit shown in FIGURE 34. Two 10 Bits DACs which are connected to a differential amplifier generate output voltages between+5/-5 V.

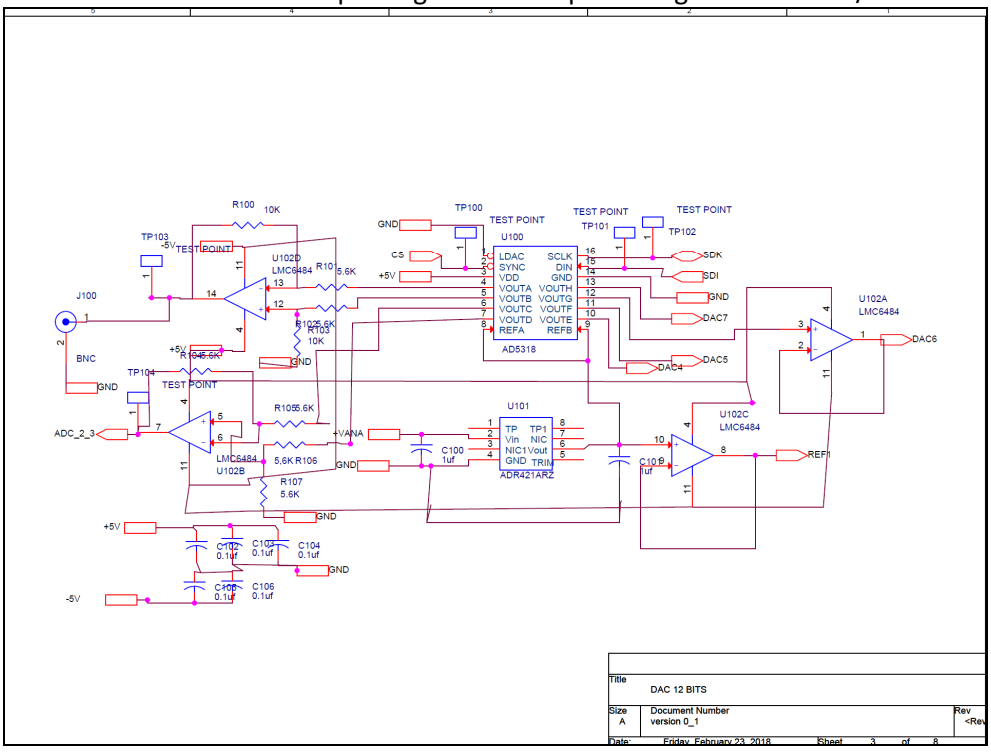

FIGURE 34. H field signal generator and other digital controlled DC sources used to drift compensation and other offset compensations.

For very low frequency measurements it will be necessary to displace the sample inside the secondary coils to reduce thermal drift. A stepper motor is used driver by an L298 directly connected to the circuit microcontroller as shown in FIGURE 35.

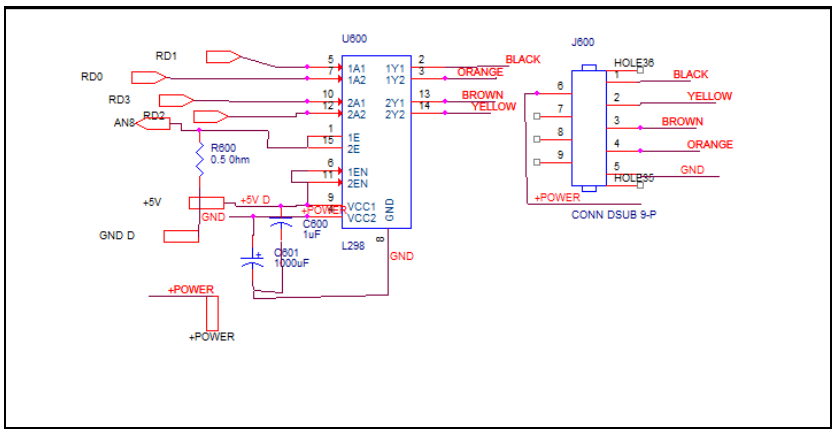

FIGURE 35. Configuration of the stepper motor to displace the sample.

Microcontroller:

FIGURE 36 shows the microcontroller that drives all the different blocks mentioned above. It has the possibility of serial communication through RS232 or RS422 to have the possibility of connecting several devices to a single serial output of the host. A 128K SPI memory has been added. FIGURE 37 shows the PCB manufactured as part of the final design stage.

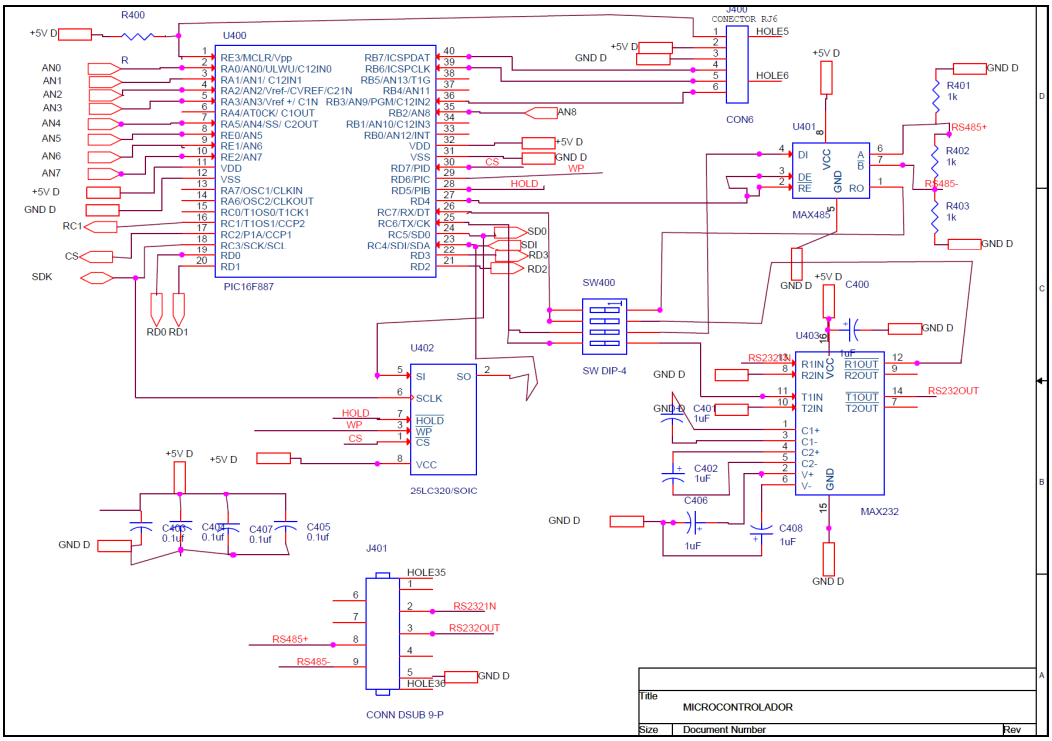

FIGURE 36. Microcontroller integrated in the control unit of the prototype 3.

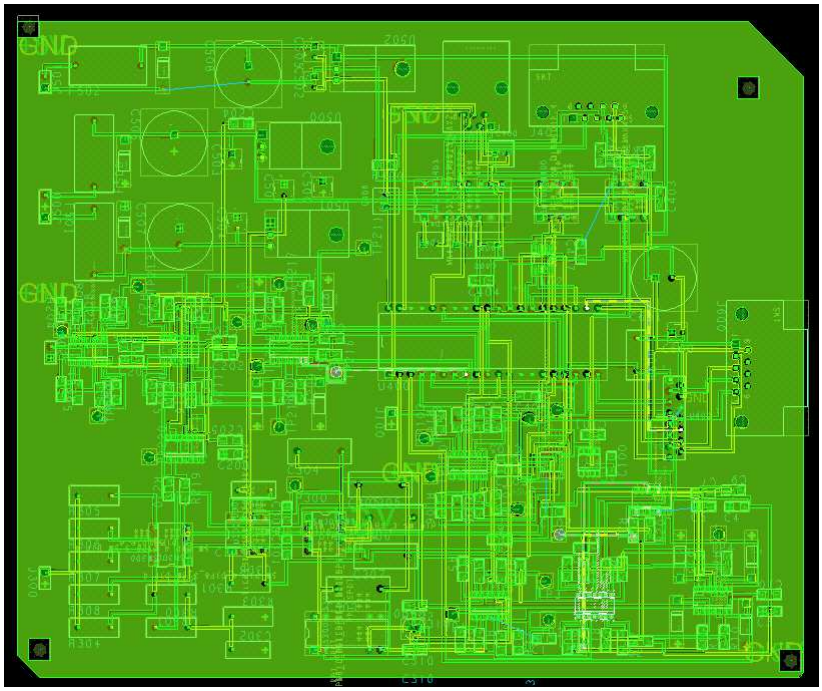

FIGURE 37. Manufactured PCB for the control unit of the prototype 3.

4.2.2. Interfaces

The control system is based in a master slave configuration. The master is a PC with windows 10 as operative system and visual net for the control consoles. In order to assure an adequate portability, the different slaves control is performance trough serial connection RS232 or RS422. The RS232 is used for some tests or in the case of a single slave. Anyway, the overall communication protocol is compatible with both serial communication systems. The communication between master and slave is based in a setup of orders (from 0 to 255) that will be executed by the slave after reception. The slave answer can be just after the execution of the order, or after the reception of the order by the slave, if the order must be executed continuously, i.e. periodic displacement of the sample, the generation of an AC signal etc. The slave always answers to the order with a head in which appears the number of the received order except in the case of error in the reception or in the execution, in both cases the answer will be the order 255 plus de number of the error.

4.2.2.1. Communications protocol

The control systems are managed from a microcontroller integrated in the own card that has code programmed, based on a series of orders that are sent through the serial interface, from a control PC or a final user application. The command protocol is based on a series of transmission frames with a fixed structure and encapsulated information so that a device (in this case a µC) can read it and extract the information it needs to execute specific code. The communication ends when the receiver of the frame answers with an ACK or confirmation of the correct reception. In the case where the receiver does not receive the frame correctly or does not understand any of the fields that compose it, it will respond with an error frame, forcing the PC to resend the frame and restart the communication.

It should be noted that the system is designed in such a way that the master of the communication will always be the PC and the slave the µC. Knowing this, the µC will always answer an order commanded by the PC, and will never start a data transmission without the PC sending it.

4.2.2.2. Structure of control frame.

FIGURE 38 shows the structure of the control frame. It is organized in: head, order, order body, error control (CRC) and tail.

FIGURE 38. Structure of the control frame.

Each of the parts is composed of fields that are fixed in the definition of the frame (are necessary for the frame to be safe and reliable). The fields are shown in more detail in FIGURE 39.

FIGURE 39. Fields that compose the control frame.

The following describes each of the fields that are part of the communication frame:

- **0x55:** This code in hexadecimal is in binary: 01010101. It has utility in detecting transmission errors or related to transmission times, delays, etc. If such a code is received well, there will be no problems associated with communication, in terms of distortions, loss of information due to problems in the channel, etc.
- **T.W (To Who):** This byte indicates to whom the message is addressed. It is the identifier of the communication receiver.
- **F.W (From Who):** This byte indicates who the message is from. It is the identifier of the communication transmitter.
- **Length (MSB):** Most significant byte of the two fields that indicate the size in bytes (within the frame) of the command and arguments. The total size will always be the number of arguments plus 1, because the order byte is implicit.
- **Length (LSB):** Least significant byte of the two fields that indicate the size in bytes (within the frame) of the command and arguments. The total size will always be the number of arguments plus 1, because the order byte is implicit.
- **Order:** Byte identifier of the command that has to execute the receiver, or that alludes to the response sent by the receiver, as well received order or request to forward the frame for that order. It can have values between 0x0 to 0xFE (inclusive). The code 0xFF is the code associated with error.
- **Arguments (from 1 to n):** Arguments associated with the order. They are usually the data that the order needs to be executed, but in the error indication frames they allude to the error that has occurred itself.
- **CRC:** Cyclic redundancy code. It is the byte resulting from the error checking function in the transmission of the frame. Generally it is usually the result of an XOR, although you can think of a more complex and reliable system.
- **0x00:** Code that marks the end of the frame.

4.2.2.3. Structure of answer frames.

There are two possible responses sent by the µC to the PC: one validation of the frame sent to start the communication and another as a negative response to said sending or error notification. The structure of both frames is shown below:

ACK frame:

FIGURE 40. Structure of the ACK frame.

In this case, as can be seen in FIGURE 40, the frame is identical to the transmission. The only change is the order of the T.W and F.W. These two bytes change the order because now the frame transmitter is the previous receiver. The advantage of sending the frame with this unique change is that the CRC is the same, so the process is remarkably simplified when checking the transmission errors.

Error frame:

FIGURE 41 shows the structure of the error frame.

FIGURE 41. Structure of the error frame.

In this case, the order field decreases to a single argument which is the error identifier. The frame notifies that an error has occurred by the order field, which becomes fixed value, 255 (0xFF) leaving the first argument of the command to indicate the particular error.

Switch on and test connection software module

This module allows establishing the connection between master and slave by pressing the button Connect, as shown in FIGURE 42. The master and slave names and port name must be given initially.

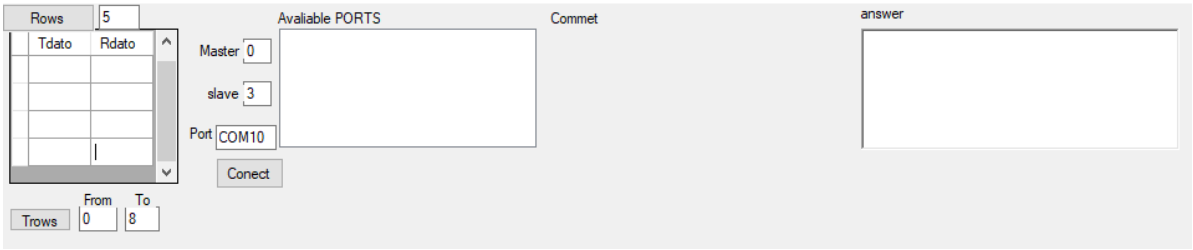

FIGURE 42. Graphical User Interface for the connection between master and slave (I).

If the selected port is not adequate, it appears the available ports and a comment suggesting the next action as FIGURE 43 illustrates.

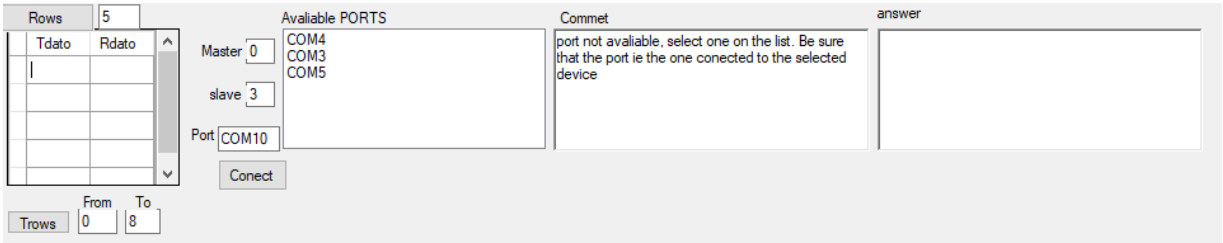

FIGURE 43. Graphical User Interface for the connection between master and slave (II).

If the slave is connected an order list appears instead of the Serial PORT selection from which an adequate one can be selected (FIGURE 44). In the left column of the grid the bytes sent to the slave appear. The answer appears in the right column. For test or to prove communications the left column can be written at any time and written bytes are sent to slave by pressing rows button.

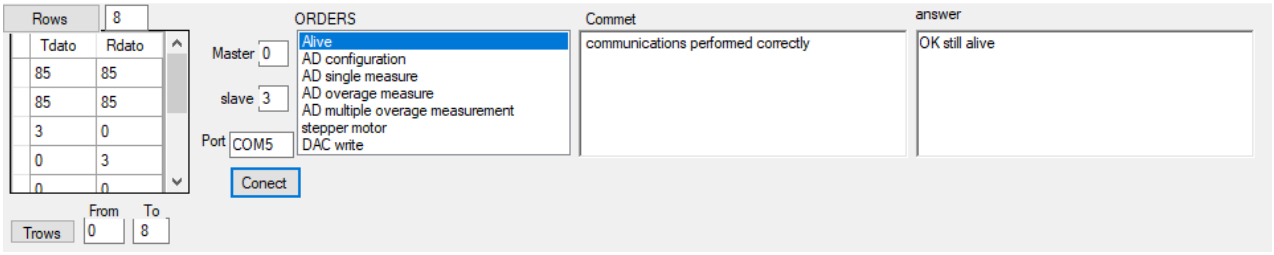

FIGURE 44. Graphical User Interface for the connection between master and slave (III).

Order control software module

Once connected, any order of the list can be selected. A grid with the parameters of the order options appears, after an adequate fulfill, the user can send the order to the slave by pressing the button "Transmit". Then the slave response is shown in the answer box and if there are data they appear in the "Received data" grid as it is shown in FIGURE 45. By presing excell button all data in the grid received data is trasfered to an Excel document.

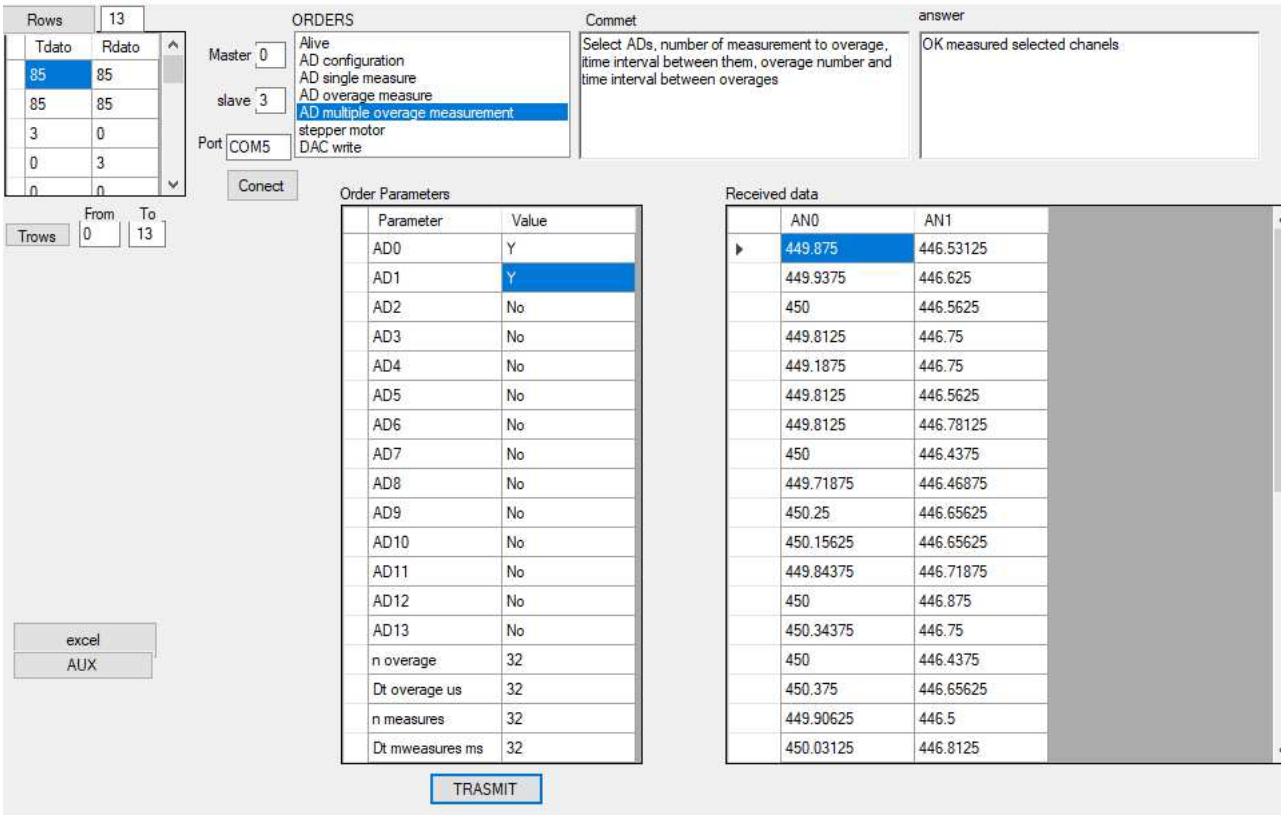

FIGURE 45. Graphical User Interface for the connection between master and slave (IV).

Microcontroller program

We have used the PIC16F887. The Microcontoller program is written in an assembler. It has the following modules:

- **Configuration module:** The data to configurate the µcontroller are stored in the EEmemory. It is divided in two sets, the first set (2100H-2180H) can be changed and stored durig executing program. To store the used configuration a security code must be used. In the second set (2180H-2200H) the initial configuration is stored to recover the original configuration. It is ussefull in the case of incorrect operation of the system. After switch-on or reset the first set is charged. Also it can be charged by an order sent by the PC. Also there is an order to store the actual configuration in the µcontroller, the orther must include a 4 bytes security number to avoid changes on initial codition made by no autorized persons. The fields inside the initial configuration are: the security number (4 bytes), the µcontroller numbe (1 byte), the used special function registers addreses and values.
- **Interruption module:** Attend to USART interruptions, SPI interruption, and timer interruption for stteper motor control. The ADCs ar contolled by poolling. If there is a frame or over run error this module send an error mensge to PC.
- **Main program:** It calls to configuration subrrutines and enter in an infinite loop, watching the state bytes and waiting for orders to execute them. The PC program sent via serial an order, and after interruption, the order is procesed by the reception module and executed by the order execution module.
- **Reception module:** After an USART interuption, this module processes and stored the received order, testing the received bytes and the parity, in case of error it sends a message with the adequate error number.
- **Order execution module:** It reads the stored received order, goes to the order subrrutine and executes the order reading the stored order body. After order execution if it is not a continuos mode, answers to the PC with data or with an acknowledge.

4.3. Implementation and validation

The control boards implemented for the NEWTON prototype 3 have been already shown in section 3. This section 3 also describes the validation tests developed to verify the functionality of the Sensor Unit. These validation tests have been developed including the control system.

5. POWER DISTRIBUTION UNIT

5.1. Overview and target requirements

The Power Distribution Unit of the NEWTON instrument supplies energy to the Control Unit and to the Sensor Unit and it is integrated by the AC current source and the power module, i.e. DC/DC converter.

With regard to the DC/DC converter, it receives the primary power from the rover and provides three different output voltages with different power consumptions which interface with the electronic CU (+5V) and the SU (±12V). The requirements of the DC/DC converter are the same for the three prototypes of NEWTON instrument, so the same design is adopted. The detail information about the final design of the DC/DC converter and its verification can be found in D3.4 [1].

Regarding the AC current source, it drives the primary winding of the Sensor Unit. The requirements of the AC current source are different for each NEWTON instrument. In the case of prototype 1 and 2 the AC current is implemented as part of the electronic Control Unit by means of using a frequency generator and an external amplifier which is placed in the Sensor Unit as D3.4 [1] and D3.5 [2]describe. In the case of prototype 3, the demand of the AC current needs and ad hoc development which is based on a Full-Bridge switching as described in the following section.

5.2. Electronic Design

We maintain the same desing shown in preliminary report D3.3 [5]. The system basically must obtain two symmetrical outputs of +-40V and a very high current, to excite the solenoid that generates the heavy magnetic field, used to drive the detection head. FIGURE 46 shows the schematic of the conversor developed for the prototype 3. The elements use in the design are: two full bridges sources, to obtain the maximal efficiency, and two transformers. Of course, all controls signals will be produced on a microcontroller system, as shown in FIGURE 47. More details related to the design of the AC current source can be found in D3.3 [5].

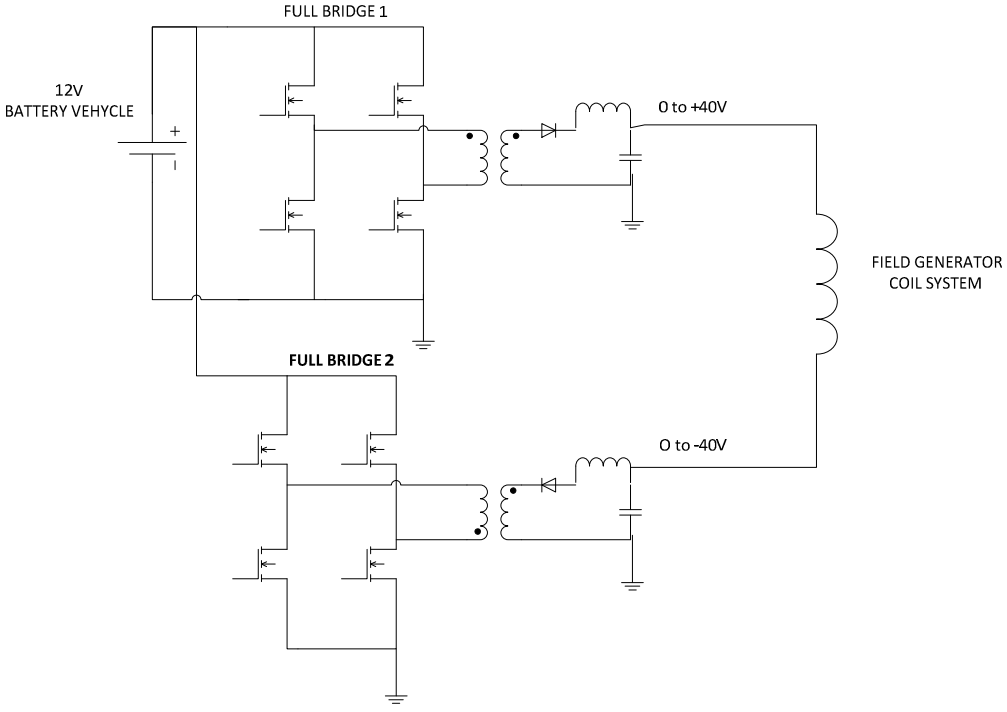

FIGURE 46. Schematic of the conversor developed for the prototype 3.

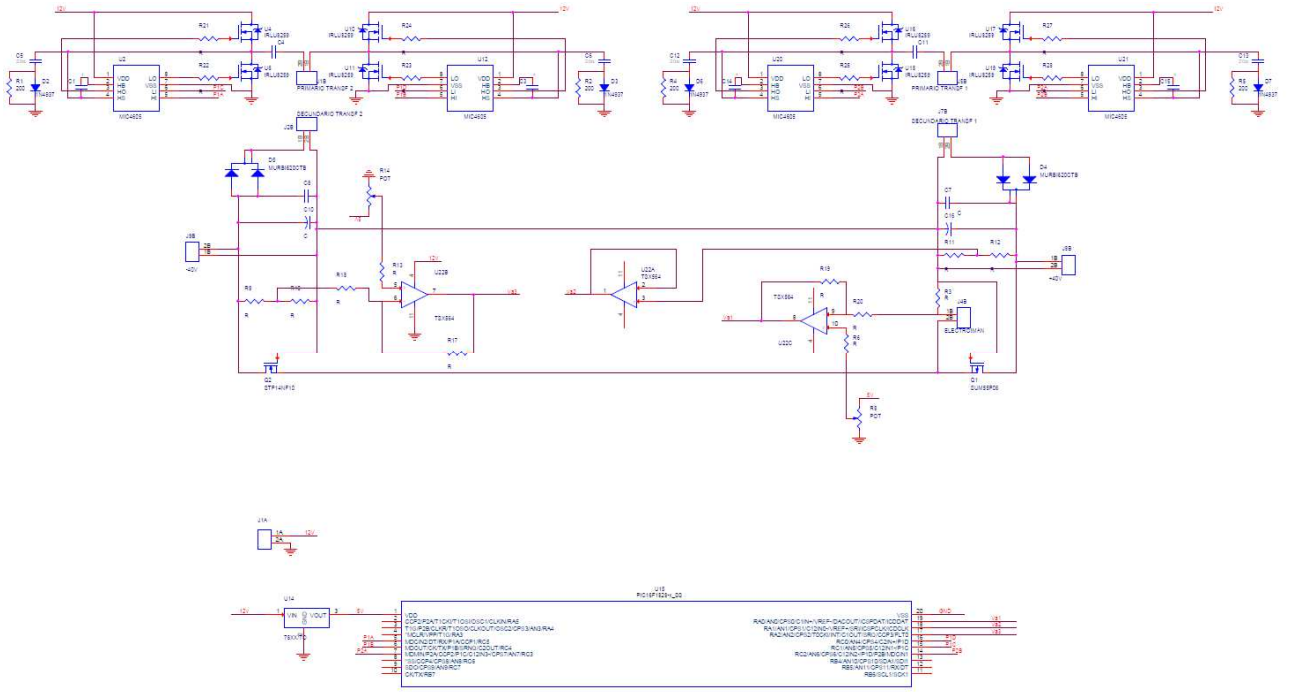

FIGURE 47. Design of the conversor including control.

5.3. PCB Manufacturing and Validation

FIGURE 48(A) shows the PCB designed for the AC current source of NEWTON prototype 3, while FIGURE 49 (B) shows the manufactured PCB. Due to a delay suffered during the manufacturing of the PCB the validation of the source has not been completed. This activitiy will be finalized during the next stage of the project and the results will be included in the following deliverable.

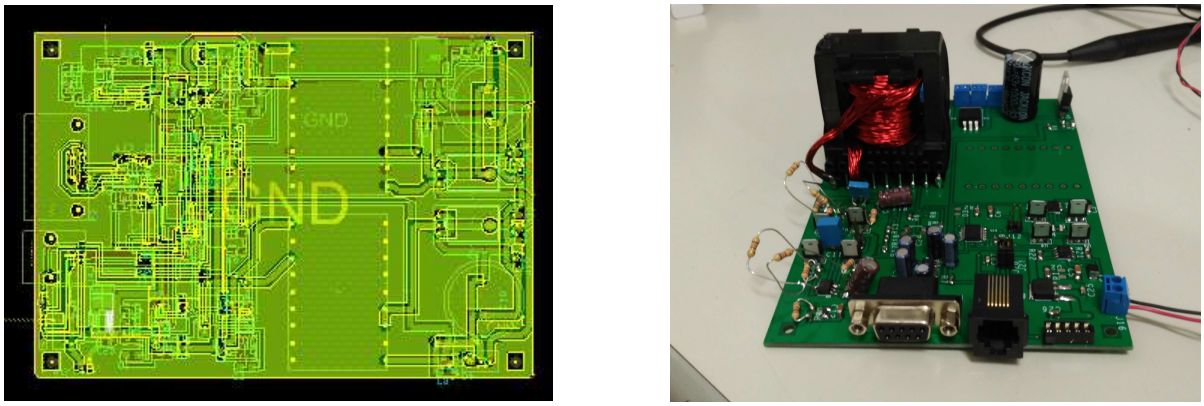

(A) (B)

FIGURE 48. (A). Board designed for the source of the prototype 3. (B) Testing prototype.

6. SUMMARY AND CONCLUSIONS

This document describes the final design of the NEWTON instrument prototype 3. The main functional blocks of this prototype are:

- **Magnetic Field Generation:**

  There are three different magnetic generators, depending on the frequencies range and the application. All of them have been built and tested with good results as follows:

  a) Ultra low frequency

  The maximum magnetic field obtained with our device is 1,2 10^5 A/m without exciting current needed. The magnetic field can be adjusted by mechanical diplacements. Therefore, this device is optimal for in-field measurements. It is also light enough to be transported when compared with the conventional electromagnets. We can obtain magnetic fields with a very good uniformity even though the intensity is slighty reduced.

  b) Low and medium frequency

  The magnetic field obtained is around $4 \cdot 10^3$ Am^{-1}/A with an uniformity better than 1%. The frequency range is from 0-12 KHz. For higher frequencies there is not a direct relation between the current given by the power source and the real current through the coil. In any case, the frequency range obtained is very adecquate to obtain magnetization curves.

  c) High frequency

  The magnetic field obtained is around $4 \cdot 10^2$ Am^{-1}/A with an uniformity of 5% in the measuring zone. The frequency range have been measured up to 130 KHz (can be higher). For this device the main problem was the heating of the coil due to high currents. We have solved this problem by designing a coil support that can be liquid cooled.

- **Magnetic Measurements**

  The system is based on an induction method and therefore, secondary coils are needed. We have designed and built up a secondary coil system based on four coils. Two of them measure the flux induced by the sample and the other two are used to compesate the remaining magnetic flux. In general, the number of turns of such secondaries must be calculated depending on the type of samples to be measured and the frequency range used. In our case we propose a design adequate for general applications with a frequency range from 0 to 50 KHz. The limit for frequency is given by the spurious capacitive that appears between turns. To process the signals from the secondary coils there are two possibilities:

  a) To integrate the signal as commonly used to obtain magnetization curves like hysteresis loop, first magnetization curves, etc. We have designed such kind of integrator with a sensitivity up to 1.2 µT/mV, depending on the secondary coil used and on the capacitance and resistance selected to perform the measurements. (A common commercial VSM minimum measurement is 6 µT of magnetization in a volume of 100 mm^3). The frequency range depends on the self induction of the secondary coil and on the selected input resistance.

  b) To directly measure it by using a lock-in amplifier. This option is commonly used to measure susceptibility vs frequency and magnetic losses. (The lock-in amplifier performance is described in D3.4 [1]).

- **Calibration**

  Taking into account that some part of the magnetic flux is lost in the secondary coils, the calibration of the system is mandatory to attain a precise measurement. Usually in induction systems, magnetic samples are used as reference for calibration purposes. We have decided to use an alternative strategy: the use of coils to simulate a magnetic specimen with a well known magnetization. This procedure allows us to calibrate the integrator directly and to calibrate the susceptibility and losses measures which results normally a very difficult task.

The design of the Sencor Unit and the electronic Control Unit of the NEWTON prototype 3 have been described in this document as well as the validation tests performed for the verification of the functionality of the blocks. With regard to the design of the AC power source, the design has been completed and the PCB has been manufactured. Due to a delay in the manufacturing of the board, the validation of this source has not been completed. This activitiy will be finalized during the next stage of the project and the results will be included in the following deliverable.

7. REFERENCES

[1] M. Díaz-Michelena et al, "Final Design Report: NEWTON instrument prototype 1 ", H2020-COMPET-2016 NEWTON - 730041, Report D3.4, April 2018.

[2] M. Sanz et al, "Final Design Report: NEWTON instrument prototype 2 ", H2020-COMPET-2016 NEWTON - 730041, Report D3.5, April 2018.

[3] M. Sanz et al, "Preliminary design report for the electronic control block ", H2020-COMPET-2016 NEWTON - 730041, Report D3.2, October 2017.

[4] M. Díaz-Michelena et al, "Preliminary design report for the magnetic head ", H2020-COMPET-2016 NEWTON - 730041, Report D3.1, October 2017.

[5] C. Lavín et al, "Preliminary design report for power distribution block ", H2020-COMPET-2016 NEWTON - 730041, Report D3.3, October 2017.